PREDICTION OF HEAT TRANSFER IN MULTIPLE GLAZE TRANSPARENCIES

Final Report

N68-22340

to

National Aeronautics and Space Administration
Manned Spacecraft Center
Houston, Texas

by

Arthur D. Little, Inc.
Cambridge, Massachusetts

August 25, 1966

Reference: NAS 9-4204

C-67248

Abstract

This report documents the results of a program to advance the techniques for evaluating the thermal behavior of window systems for space vehicles, particularly those exposed to the environmental conditions attendant to planetary re-entry.

The report is presented in three complementary parts. The first part outlines the purpose and scope of the program, summarizes its major results, and presents the contributors conclusions and recommendations. The second part describes the theory and mathematical models applied to the solution of the problem of heat transfer in observation window systems typical of those applicable to re-entry type spacecraft. The third part presents the methods and results of tests to examine the validity of the developed computer program to simulate the thermal behavior of spacecraft window systems operating in severe thermal environments.

Foreword

This work is sponsored by the National Aeronautics and Space Administration in order to improve the presently available means to determine the thermal behavior of semitransparent windows. NASA's interest centers on the use of window materials in spacecraft--both for human and instrument observation. The structural integrity of window systems subjected to adverse thermal environments, especially those attendant to planetary re-entry, is one issue which sponsors the inquiry. The transport of heat from the environment through the window system is another.

The thermal environment expected by spacecraft window systems during re-entry is severe. Instantaneous and time variations in heat flux from the environment via convection and radiation mechanisms are extremely large compared with common engineering experience. At the same time, the demands for precise knowledge of the thermal behavior of the windows is augmented by the very nature of their use. Accordingly, this work is directed to build on the existing scientific and engineering background on the subject.

Contract NAS 9-4204, administered by the Manned Spacecraft Center, Houston, Texas, provides this summary report of all work directed to the use of a computer simulation to predict the behavior of multiple pane windows for use in spacecraft of the near future. In addition, as part of this contract, a manual of instruction to potential users of the developed computer program is issued under separate cover.

Technical administration of the contractor's work was under the direction of Mr. Robert S. Harris, Jr., Manned Spacecraft Center, Thermo-Structures Branch, National Aeronautics and Space Administration, Houston, Texas.

Acknowledgments

This work has been carried out under the direction of Mr. Arthur A. Fowle.

Mr. Peter Strong conceived the analytical approach and translated it into a useful computer program with the major assistance of Mrs. Carol H. Sox.

Mr. Daniel Comstock, Mr. John McCullough, and Mr. Edward Boudreau were major contributors to the design, execution, and evaluation of the experimental phases of this program.

Table of Contents

PRECEDING PAGE BLANK NOT FILMED.

List of Figures

PART 1

SUMMARY

I. PURPOSE AND SCOPE

The objective of this program has been to develop improved methods for evaluating the thermal behavior of observation windows for use in planetary re-entry vehicles. The work includes: 1) an analysis of the thermal behavior of multiple-glaze window systems operating under conditions typical of those attendant to planetary re-entry, 2) the development of a computer program for predicting this behavior, and 3) an experimental program to test the validity of the predictive techniques developed.

This report documents the results of all work completed under this program. A complementary report entitled, "A Computer Program for the Prediction of Heat Transfer in Multiple Glaze Transparencies: A Users Manual," dated 25 August 1966, also results from this effort.

II. RESULTS

A computer program for simulating the thermal behavior of window systems in extreme thermal environments has been developed. The analysis providing the basis for this computer program is presented in Part 2 of this report. Part 3 describes in detail the experimental program carried out to test the ability of the computer program to predict the behavior of windows under conditions of interest.

The measure of success attained in meeting the objectives of this program is best demonstrated by comparisons between the predicted and the measured thermal performance of sample windows tested under controlled experimental conditions. To this purpose tests were carried out in this program (ADL tests) on quartz, aluminosilicate and gold-coated quartz window samples in the form of disks 0.635 cm thick and 6.35 cm in diameter. These samples were placed in an evacuated chamber with water cooled walls. The chamber also contained a resistant-heated graphite cavity as a source of high temperature thermal radiation. Provisions were made for the sudden exposure of the window samples originally held at near ambient temperature levels to the source. The samples were instrumented on both faces with gold film temperature sensors and measurements of temperature vs. time were recorded as the samples were heated. Measurements of the total thermal irradiance leaving the back surface of the window samples were made also.

Computer predictions were also compared with the results of two experiments carried out by Midwest Research Institute (MRI) and reported in reference 3. The first experiment involved an instrumented 96 percent silica window disk convectively (torch) heated at one surface in a room environment. The convective heat flux per unit area, the temperature on both faces of the sample, and the net flux per unit area leaving the unheated face of the sample were measured at steady state. The second experiment involved the cooldown of an originally heated window

sample in a room environment. Window surface temperature was measured as a function of time.

Table I summarizes the conditions of all experiments used to test the validity of the developed computer program. Figures 1 through 6 illustrate laboratory test results and compares them with those predicted by computer simulations.

The results of computer runs made in order to check the function of the computer program when programmed to handle window systems with multiple panes and reflective coatings are shown in Figures 7 and 8.

Figures 9 and 10 depict the results of laboratory experiments conducted to verify the ability of the computer program to predict the behavior of windows with reflective coatings. This objective was not attained for the reflective properties of the gold film were destroyed in calibration tests and computer simulations were not attempted.

Examination of Figures 1 through 6 reveals that the difference between all measured and predicted temperatures never exceeded five percent of the average of the measured and predicted temperatures. The measured temperatures in tests completed in this program were with few exceptions higher than the predicted values. The fact that the measured temperatures in ADL tests were consistently lower than the predicted temperatures and the degree of this disparity is explained (in Part 3) mainly by the non one-dimensional character of the heat transport in the test window samples engendered by the test conditions. Any residual difference not explained on this basis lies within the uncertainty interval of the measured temperatures.

The difference between measured and predicted values of the hot face temperatures minus the cold face temperatures of the test window

TABLE I
SUMMARY OF TEST CONDITIONS

ADL TEST AND COMPUTER SIMULATIONS

Test Sample	Sample Thickness (cm)	Sample Diameter (cm)	Cavity Temperature (^{0}K)	Sample Location (Distance from Cavity Aperture) (cm)	Surrounding Temperature (^{0}K)	Test Conditions	Reference Figure No.	Reference Experiment Number
Fused Silica (Quartz)	0.635	6.35	1137	3.60	300	Sudden Irradiation from Black Body Cavity Source in Vacuum Black Cooled-Wall Surroundings	1	45
			1380		300		2	46
Aluminosilicate	0.635	6.35	1123	3.20	300		3	51
			1303		300		4	52
Quartz with Gold* Film	0.635	6.35	1147	3.60	300		9	48
			1302		300		10	49

*Reflecting properties of gold film destroyed in calibration tests. No computer simulation attempted.

MRI TESTS AND ADL COMPUTER SIMULATIONS

Test Sample	Sample Thickness (cm)	Sample Diameter (cm)	Thermal Energy Source	Ambient Temperature (^{0}K)	Test Conditions	Reference Figure No.	Reference Computer Run
96% Silica	0.795	5.08	Convective heat flux directed to one face equal to 3.7 watts/cm^2	294	Steady state forced convective heating of one surface of sample in room air surroundings. Other surface faces a cooled calorimeter spaced 0.444 cm from it. Cooldown in room air from 770^{0}K	5	ADL Run 60
				294		6	ADL Run 60

ADL COMPUTER TEST SIMULATIONS ONLY

Test Sample	Sample Thickness (cm)	Sample Diameter (cm)	Cavity Temperature (^{0}K)	Sample Location (Distance from Cavity Aperture (cm)	Surrounding Temperature (^{0}K)	Test Conditions	Reference Figure No.	Reference Computer Run
Quartz with Gold Film	0.635	-	1310	3.60	294	Sudden Irradiation from Black Body Cavity in Vacuum Black Cooled-Wall Surroundings.	7	ADL Run 4
90% Silica + Aluminosilicate	0.635 (each)	-	1900	96% Silica at 3.60 cm aluminosilicate placed behind & parallel, close but not touching.	294		8	ADL Run 2

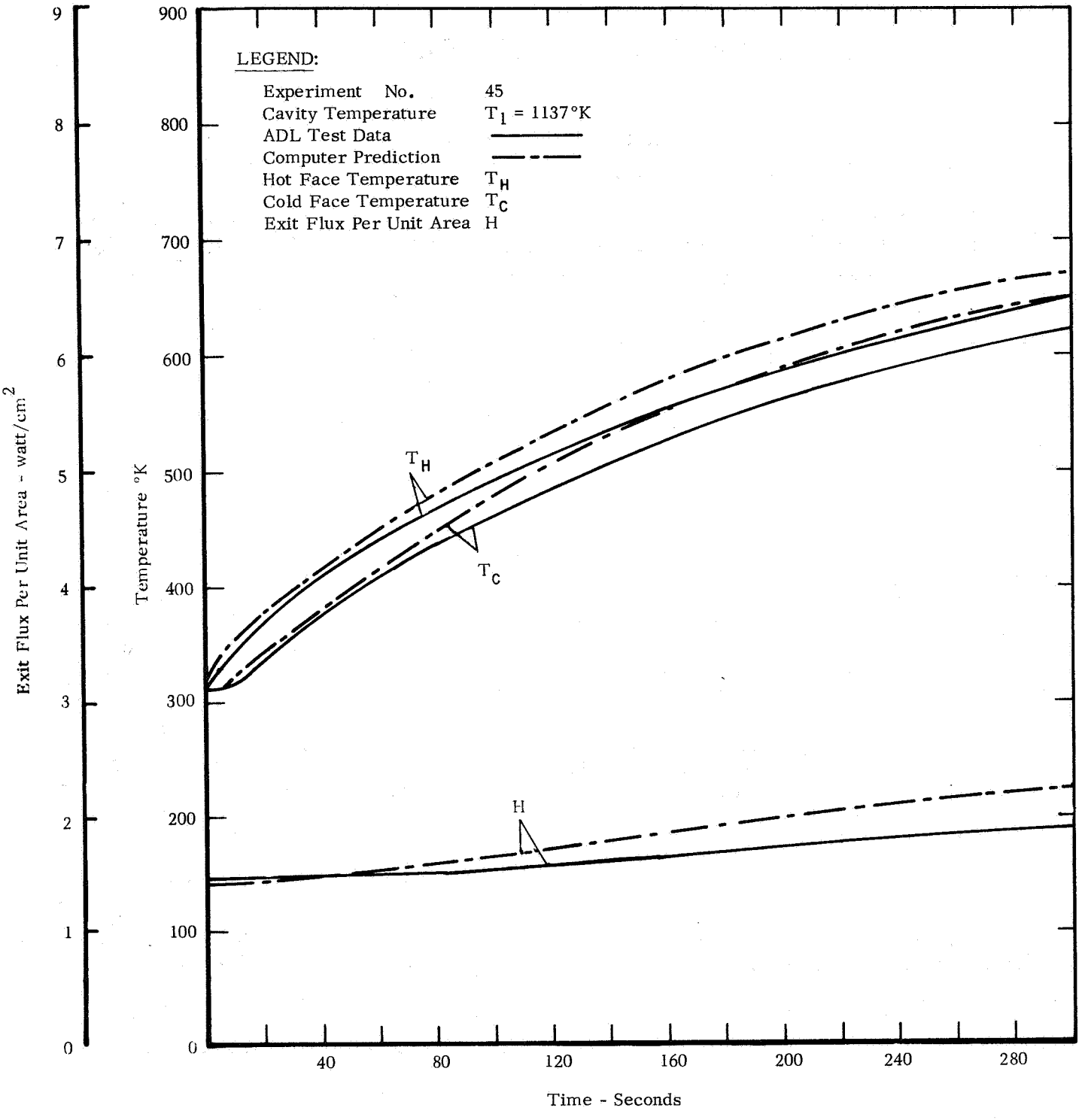

FIGURE 1 COMPARISON OF ANALYTICAL AND EXPERIMENTAL RESULTS -- QUARTZ

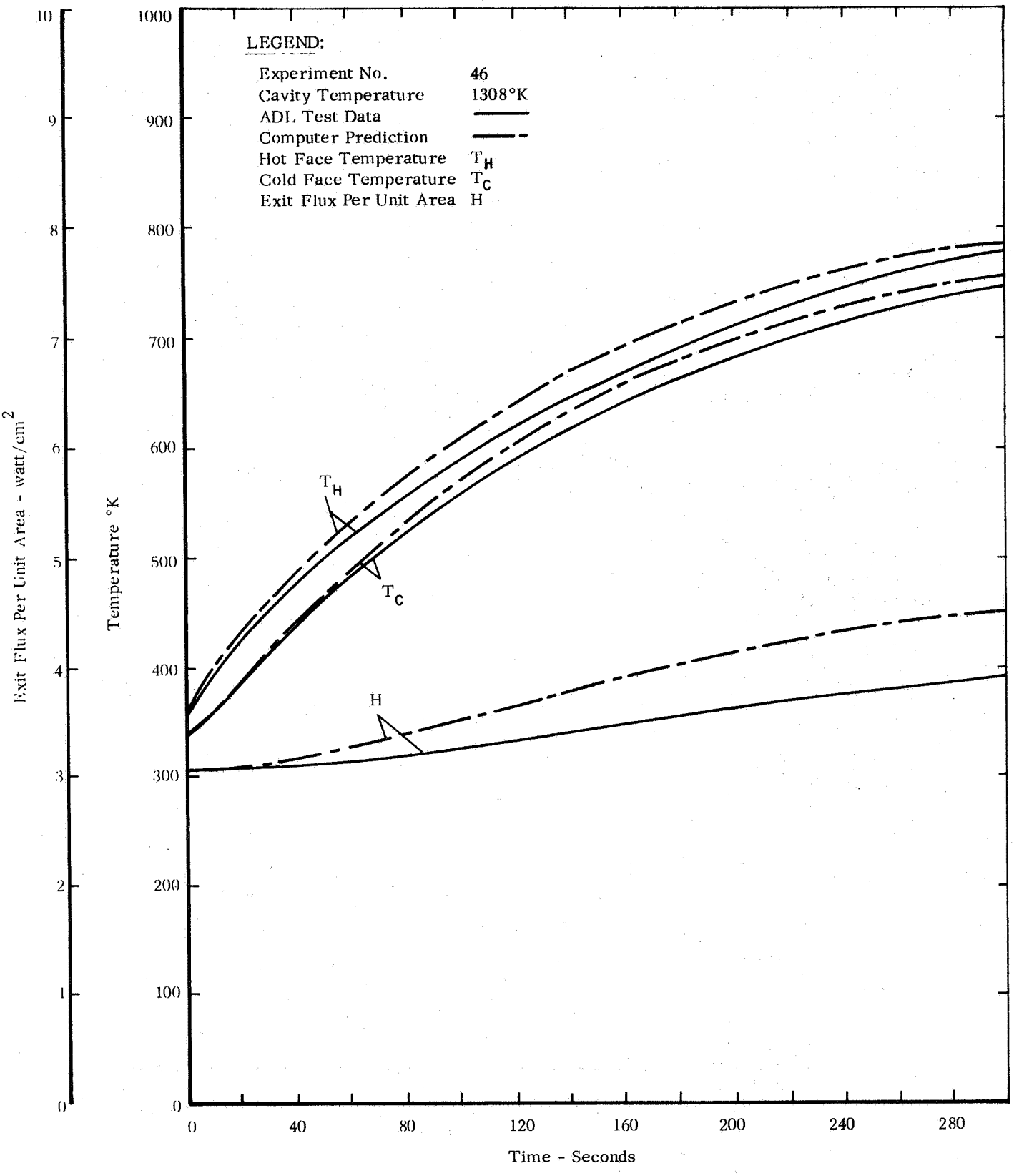

FIGURE 2 COMPARISON OF ANALYTICAL AND EXPERIMENTAL RESULTS -- QUARTZ

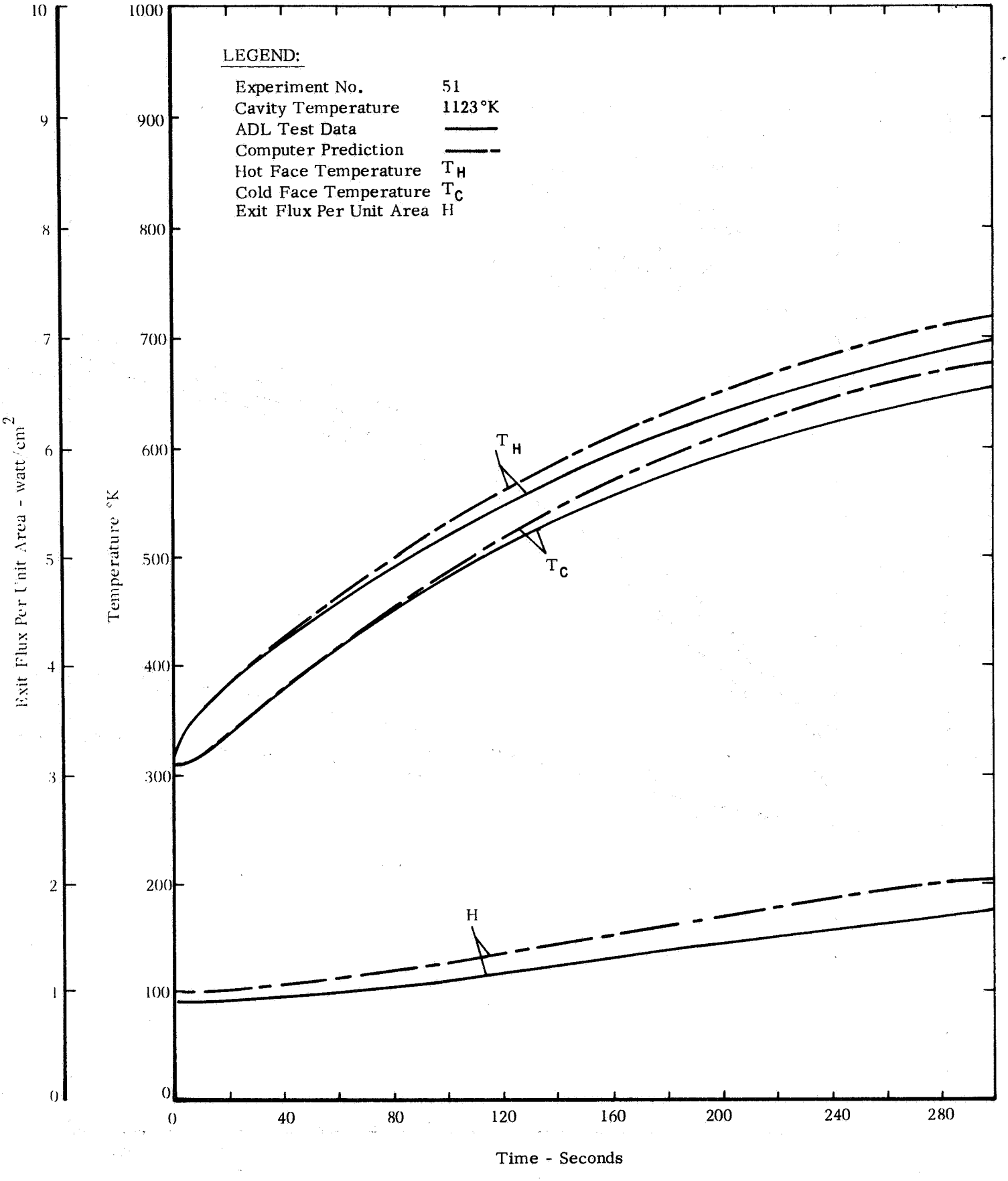

FIGURE 3 COMPARISON OF ANALYTICAL AND EXPERIMENTAL RESULTS -- ALUMINOSILICATE

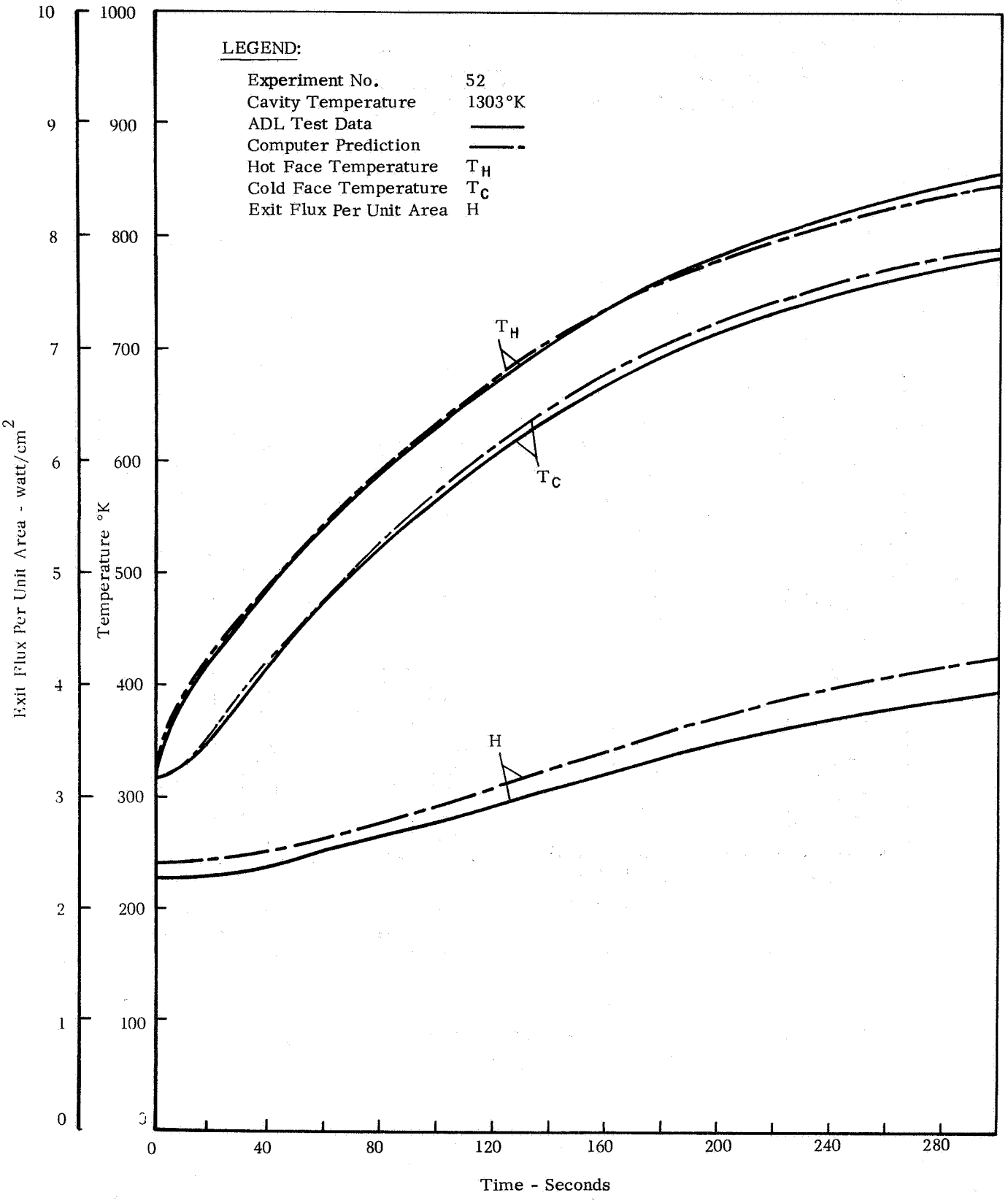

FIGURE 4 COMPARISON OF ANALYTICAL AND EXPERIMENTAL RESULTS -- ALUMINOSILICATE

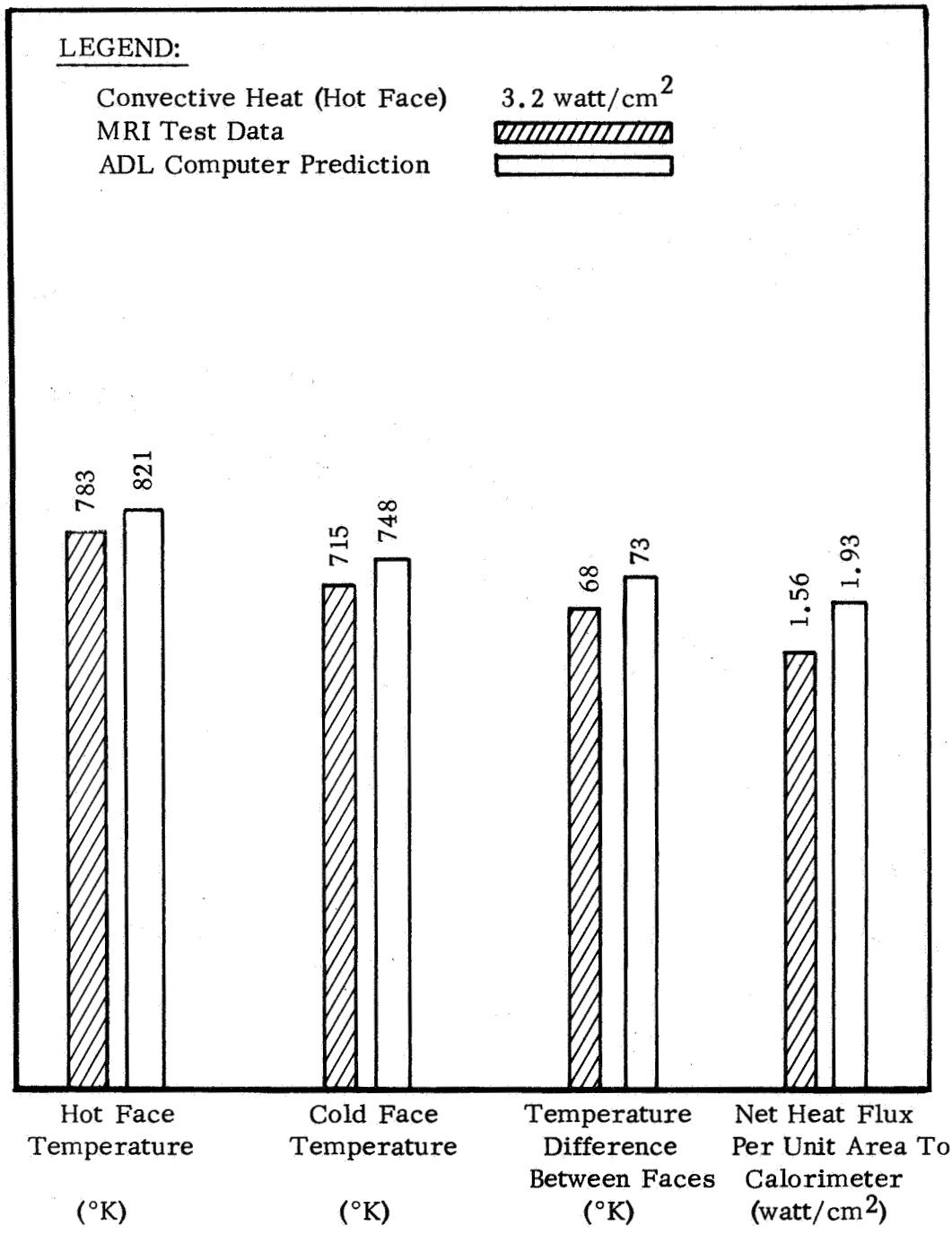

FIGURE 5 COMPARISON OF ANALYTICAL AND EXPERIMENTAL RESULTS -- 96% SILICA

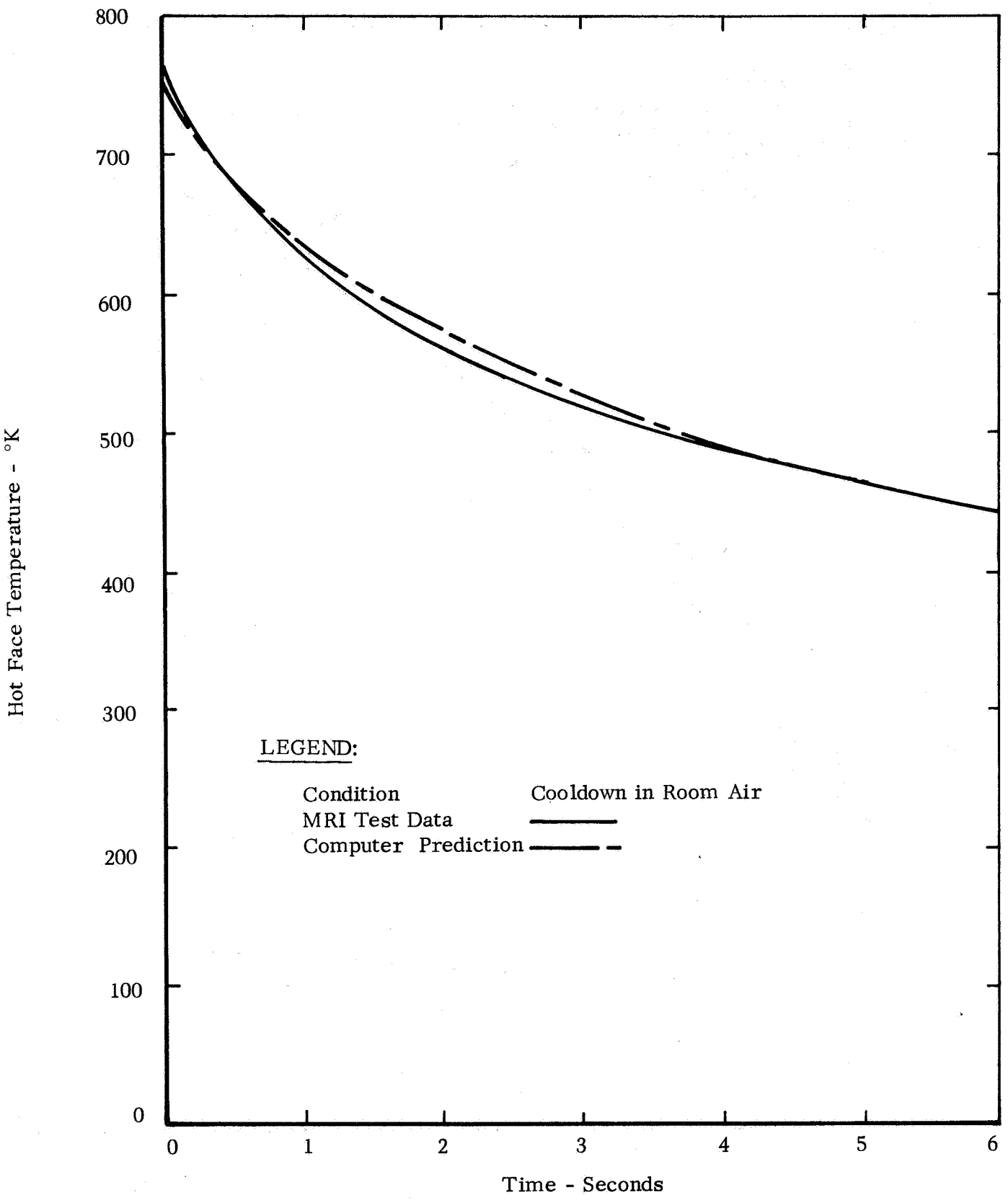

FIGURE 6 COMPARISON OF ANALYTICAL AND EXPERIMENTAL RESULTS -- 96% SILICA

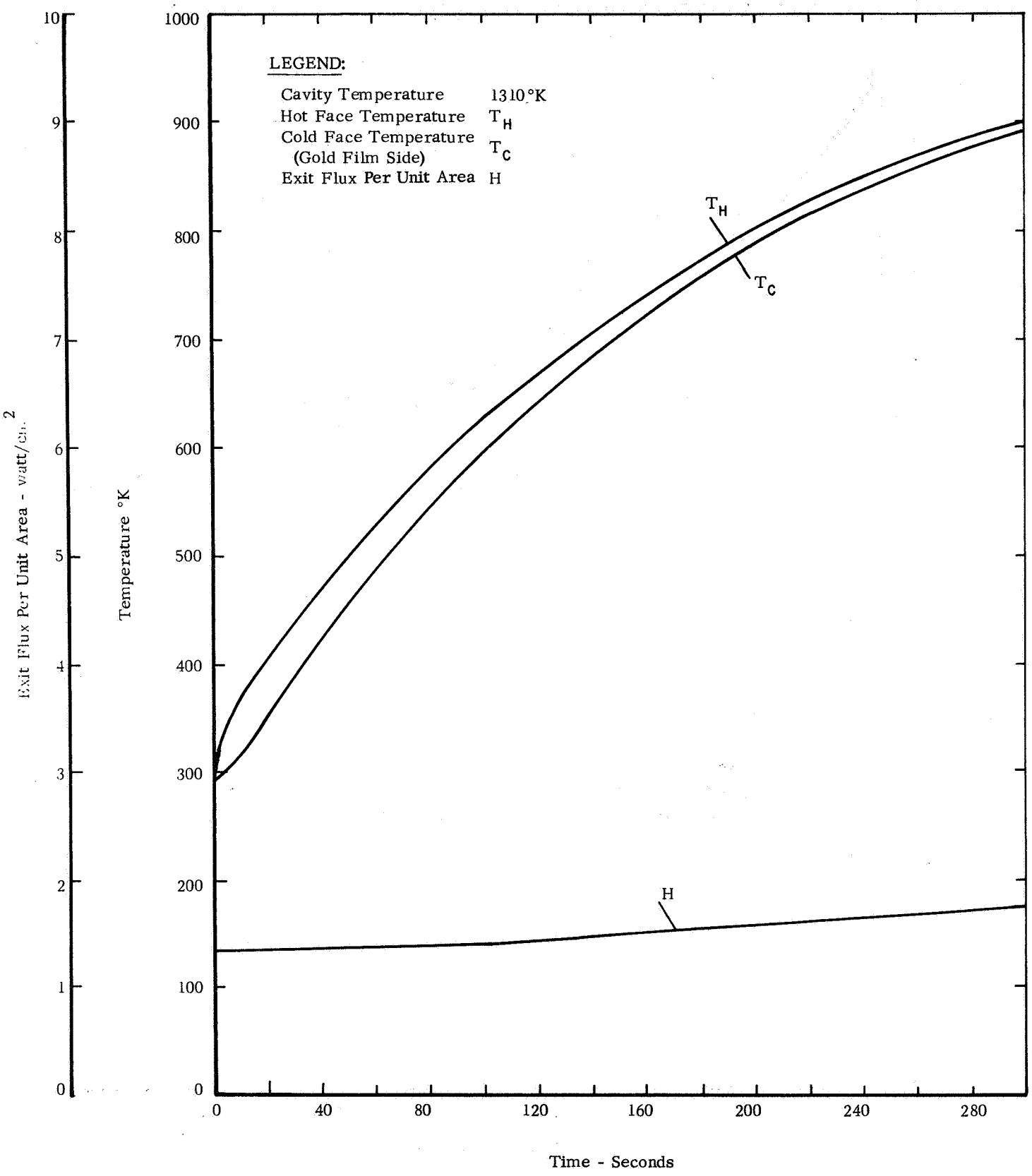

FIGURE 7 COMPUTER TEST SIMULATION -- QUARTZ + GOLD FILM

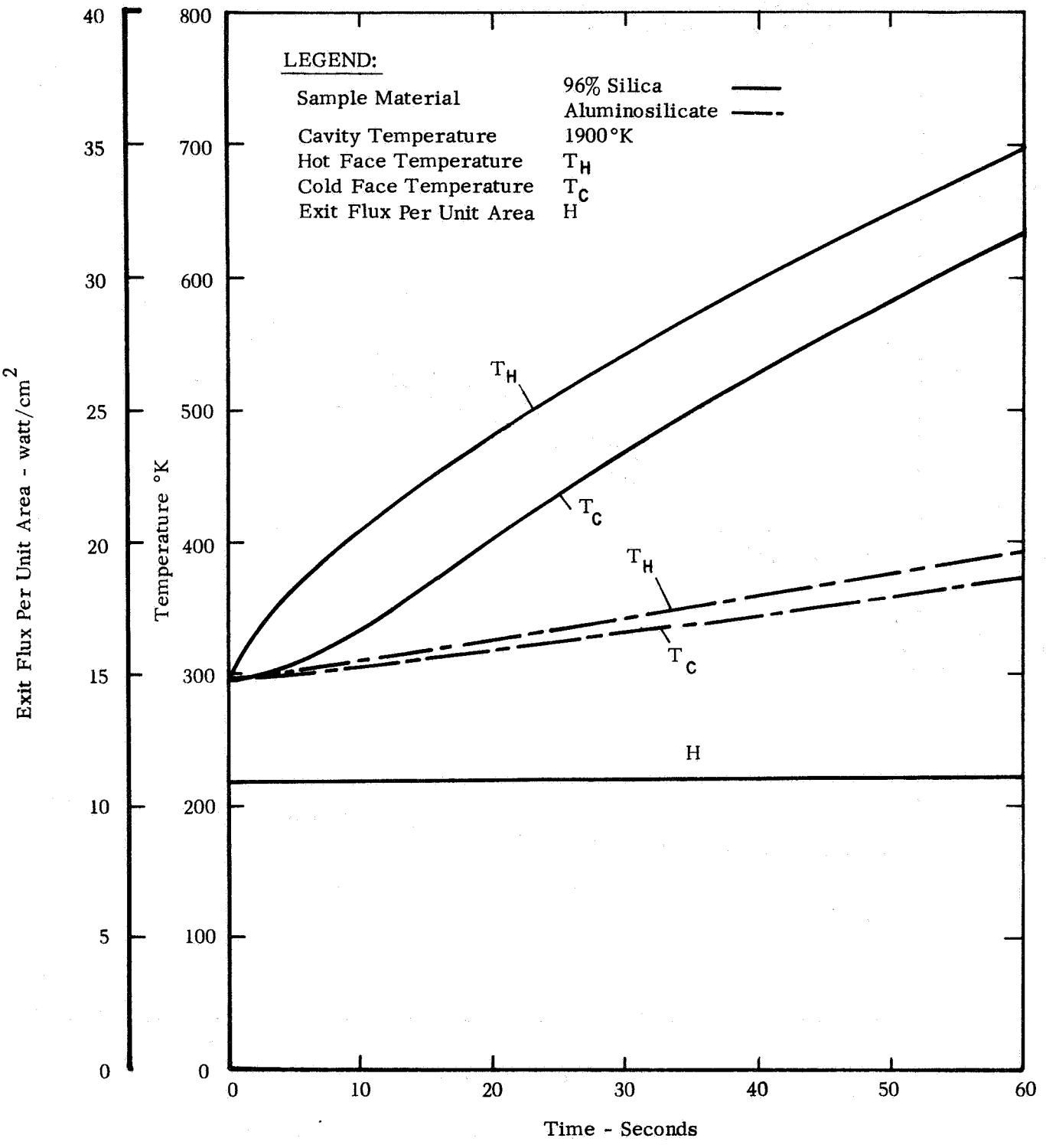

FIGURE 8 COMPUTER TEST SIMULATION -- 96% SILICA AND ALUMINOSILICATE

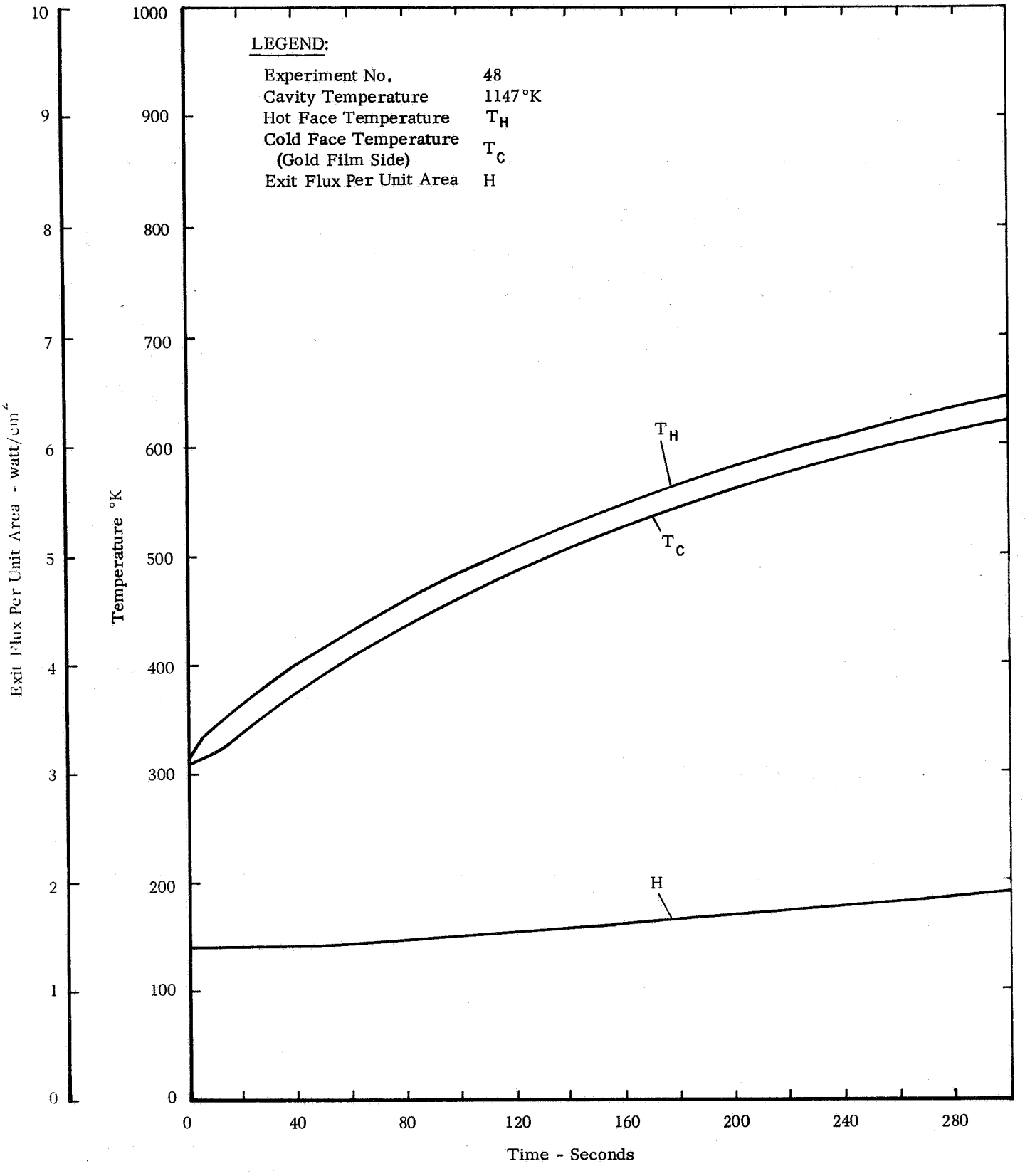

FIGURE 9 EXPERIMENTAL RESULTS -- QUARTZ + GOLD FILM

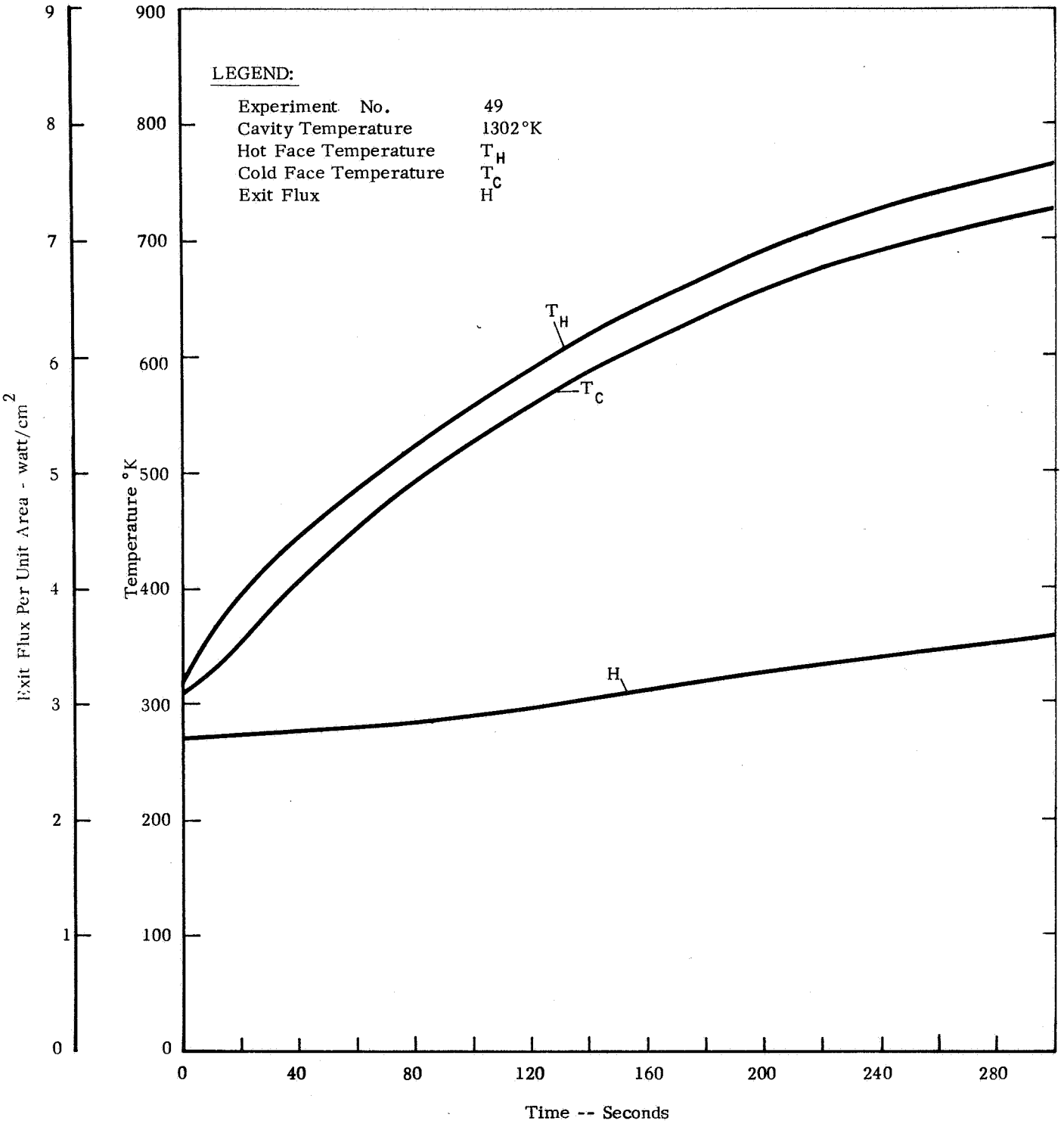

FIGURE 10 EXPERIMENTAL RESULTS -- QUARTZ + GOLD FILM

samples never exceeded 30 percent of the average of the measured and predicted values. In all but one out of five tests this difference was never more than 15 percent. The differences between measured and predicted values are spanned by the uncertainty intervals of the measured temperatures; however, the case of the 30 percent difference may be best considered a point on the statistical fringe of the uncertainty interval.

Again, examination of Figures 1 through 6 shows that the difference between the measured and predicted thermal flux per unit area leaving the back (cold) face of the test window samples never exceeded 19 percent. The discrepancy between predicted minus measured fluxes in ADL tests is consistently positive. This fact is in agreement with and is explained in about half measure by the non one-dimensional character of the heat transport in the window samples under test conditions. In addition, the measurements of the thermal flux leaving the test window samples shown in Figures 1 through 4 are estimated to be some few percent lower than the actual values because of identifiable reasons explained in Part 3.

Figures 5 and 6 appear in strong support of the validity of the developed computer program to handle problems of heat transport in semi-transparent glazings with convective as well as radiant heat transport at boundaries.

Figure 7 is produced as evidence of the ability of the computer program to handle windows with reflective coatings. The computer test case involves a quartz window with a reflective gold film with a pass band in the visible spectra. The results of Figure 7 are to be compared to Figure 2. Qualitatively the differences are in order. The gold film sample is less transparent than the uncoated quartz, and this fact shows in the lower value of the thermal flux leaving. Consistent with this fact the temperature levels are higher and the temperature differences between the hot and cold surfaces of the test sample are reduced.

Figure 8 illustrates the ability of the computer program to simulate the thermal behavior of multi-glaze samples. The results are compatible with certain arguments based on physical reasoning. For instance, the temperature of the aluminosilicate window rises comparatively slowly for the incident energy from the source, filtered by the 96 percent silica window, lies primarily in its transparent band. The thermal flux leaving the aluminosilicate window is due almost entirely to that transmitted through the two panes in their semi-transparent bands and is therefore nearly constant for the duration of the test period. The magnitude of the transmitted flux is in agreement with simple first order calculations. From these and similar observations we believe that the computer program adequately simulates the behavior of multi-pane window systems.

Figures 9 and 10 show the results of laboratory tests meant to test the behavior of a window sample with a reflective gold film. In fact, the reflective properties of the gold film were destroyed during calibration runs and for all practical purposes the window behaved as if it were clear quartz. Subsequent measurements of spectral transmittance and reflectance on this test sample when compared with those of a clear quartz confirmed this fact.

III. CONCLUSIONS AND RECOMMENDATIONS

The developed computer program is a useful tool for predicting the thermal behavior of multi-glaze window systems, particularly in the thermal environments attendant to planetary re-entry. The agreement between experimental data resulting from validation tests and computer predictions is good. In fact, the disparity between the results of computer simulations and corrected test data have not proved large enough nor consistent enough to reveal any basic inadequacy in the computer program.

The developed computer program is an extremely detailed representation of the thermal behavior of window. This detail reflects in a demand for input data and computer running costs. The computer program runs at a 3.6 to 1 ratio to real time on an IBM 7090, so computer costs are not excessive even though no attempt has been to find the optimum balance between numerical accuracy and computing time. On the other hand input data having the detailed structure that can be handled by the computer program is difficult to provide. For this reason, it would be useful and instructive to test the effect of various kinds and degrees of simplification of input data on the predicted results.

PART 2

ANALYSIS

I. INTRODUCTION

In this section we describe an analysis for determining the temperature distribution in multiple glazing systems as a function of position and time. The method used accounts for both radiation and conduction in the glass slabs, radiation and convection in the spaces between the slabs, and reflected and transmitted radiation at surface coatings. Variations in thermal conductivity and heat capacity of the window materials as a function of temperature and variations in certain optical properties as a function of wavelength, temperature and angle are accommodated. It is assumed that the temperature is a function of only a single coordinate perpendicular to the slab.

II. THEORY OF HEAT TRANSFER THROUGH SEMITRANSPARENT CONDUCTING SLABS

A. INTERIOR POINTS

At high temperatures both phonon conduction and the absorption and emission of radiation are important contributors to the transport of heat in glasses. Therefore, the usual diffusion equation governing heat flow must be extended to include the effects of radiation. We will develop this extension for the case in which the temperature is a function of only a single coordinate, say x, perpendicular to the slabs. We will use a generalization of Schuster's two-beam method[21]* to account for the radiative transfer in the wavelength region in which the glass is semitransparent. In the wavelength region in which the glass is opaque, the radiative effects can be ignored.

Figure 11 shows an element of thickness dx in the interior of a slab with two rays of intensities $I(x,\theta,\lambda)$ and $J(x,\theta,\lambda)$ traversing the element in opposite directions at an angle θ with respect to the x-axis. Here λ is the wavelength in microns, and the intensity is given in units of watts-cm^{-2}-steradian^{-1}-micron^{-1}.

The intensities I and J vary with distance, s, along the rays according to the equations

$$\frac{\partial I}{\partial s} = \alpha\,(E-I) \qquad (1)$$

$$-\frac{\partial J}{\partial s} = \alpha\,(E-J) \qquad (2)$$

where

$\alpha = \alpha\,(\lambda,T)$ is the absorption coefficient (cm^{-1}) at the wavelength λ and temperature T(°K)

E is the intensity of emission (watts-cm^{-2}-steradian^{-1}-micron^{-1})

* Numbers in parentheses refer to references listed in Appendix C at end of report.

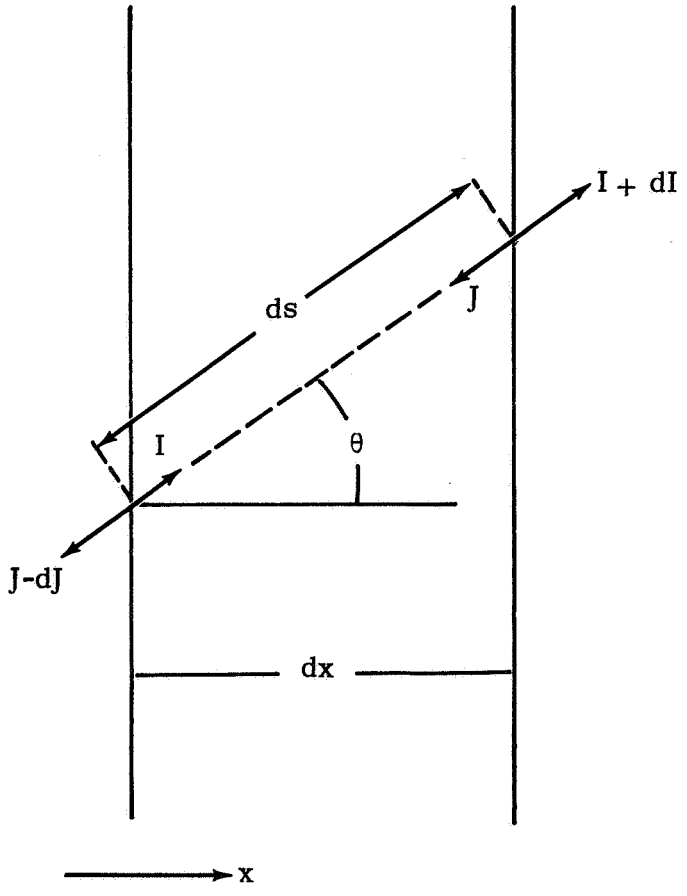

FIGURE 11 ILLUSTRATION FOR RADIANT HEAT TRANSFER ANALYSIS

The intensity of emission depends on the Planck radiation function and the index of refraction, n, according to the relation

$$E = \frac{n^2}{\pi} B(\lambda,T) = \frac{n^2}{\pi} \frac{C_1}{\lambda^5\left(e^{C_2/\lambda T}-1\right)} \tag{3}$$

Equations 1 and 2 can be transformed to depend on x rather than s by making the substitution

$$dx = ds \cos\theta \tag{4}$$

so that

$$\cos\theta \frac{\partial I}{\partial x} = \alpha (E - I) \tag{5}$$

$$-\cos\theta \frac{\partial J}{\partial x} = \alpha (E - J) \tag{6}$$

Equations 5 and 6 represent a doubly infinite set of equations covering all angles and wavelengths. In practice a number of simplifying assumptions and approximations must be made in order to obtain a solution. In the first place, the material is characterized by two well-defined spectral regions. In one region (the opaque region) α is very large, and therefore E = I and no significant heat transport by radiation occurs; thus the intensities I and J need not be calculated in this wavelength region. In the other region (the semitransparent region) Equations 5 and 6 must be solved, but one considers a small number N of conical beams at various angles and a small number M of wavelengths. Also one restricts the number P of places in the slabs at which the intensities are calculated. Thus 2MNP intensities must be computed for each value of the time. Unfortunately for even quite modest values of M, N, and P (for example, M = 30, N = 4, P = 20, which are the numbers chosen in the program to be described) the number 2MNP may be prodigious (4800 in the present example).

In Equations 5 and 6 the temperature T is a variable which must be calculated from the diffusion equation which has been generalized

to include the effects of radiation. This equation is

$$C\rho \frac{\partial T}{\partial t} = \frac{\partial}{\partial x}\left(K \frac{\partial T}{\partial x}\right) + \iint \alpha (I + J - 2E)\cos\theta d\omega d\lambda \qquad (7)$$

where

$C\rho$ is heat capacity, joules $cm^{-3}(°K)^{-1}$

K is thermal conductivity, watts $cm^{-1}(°K)^{-1}$

$d\omega$ is an element of solid angle, steradians

t is the time, seconds.

It has already been noted that α is a function of the temperature, and so are C and K. The integration over the solid angle extends over a hemisphere, and the integration over wavelength extends over the semi-transparent spectral band.

Equation 7 and the set of equations of the form of Equations 5 and 6 are all that are needed to describe the variation of temperature and intensity of radiation at interior points.

B. BOUNDARY CONDITIONS

In order to find a unique solution to the set of differential Equations 5, 6, and 7 it is necessary to prescribe certain conditions that must be satisfied at the boundaries of the slabs. In addition to the usual conditions regarding the temperature and its normal derivative, the external radiation intensity I_e must be specified on the left-hand side and the external radiation intensity J_e must be specified on the right-hand side. Both intensities must be specified as functions of the angle, wavelength, and time. It is to be noted that the number of incoming beam intensities to be specified at a boundary is less than the number MN of beams traveling in the incoming direction just inside the boundary because entering beams are refracted into a cone of half-angle less than $\pi/2$ (actually, about $\pi/4$ in glass), while some of the interior beams suffer total internal reflection. The complete boundary condition on I at the left-hand side of a slab is

$$I = (1 - R)I_e \frac{\cos\theta_e}{\cos\theta} \frac{d\omega_e}{d\omega} + RJ \tag{8}$$

where

R is the reflection coefficient as a function of angle and wavelength

$\frac{d\omega_e}{d\omega}$ is the ratio of infinitesimal solid angles occupied by the external and corresponding internal beams

θ_e is the angle of the beam outside the glass

The angles θ and θ_e are related by Snell's law

$$n \sin\theta = \sin\theta_e \tag{9}$$

Hence it can be shown that

$$\frac{\cos\theta_e}{\cos\theta} \frac{d\omega_e}{d\omega} = n^2 \tag{10}$$

Thus the boundary condition becomes

$$I = (1 - R)n^2 I_e + RJ \tag{11}$$

The intensity of the left-hand external emergent beam, J_e, can also be calculated from I_e and J by the formula

$$J_e = (1 - R)\frac{J}{n^2} + RI_e \tag{12}$$

Clearly Equation 12 applies only to those beams which are not totally internally reflected. For the totally internally reflected beams the boundary equations are merely

$$I = J \tag{13}$$

$$J_e = 0 \tag{14}$$

At the right-hand boundary of a slab, the conditions on the penetrating beam intensities are

$$J = (1 - R)n^2 J_e + RI \tag{15}$$

$$I_e = (1 - R)\frac{I}{n^2} + RJ_e \tag{16}$$

Again, for the totally internally reflected beams the boundary equations are

$$J = I \tag{17}$$

$$I_e = 0 \tag{18}$$

In these last four equations I_e is the intensity of the emergent beam and J_e is the prescribed intensity of the incident beam.

It is important to calculate the intensities of the emergent beams because in multiple pane systems the beam emergent from one pane is incident on the next pane and so on. Furthermore it is necessary to calculate the flux that enters the cabin through the window system.

In our work we have assumed that polarization effects are negligible. In case the surface of the slab is uncoated, we assume that the intensity reflection coefficient R is given by the Fresnel formula

$$R = \frac{1}{2}\frac{\sin^2(\theta_e - \theta)}{\sin^2(\theta_e + \theta)}\left\{1 + \frac{\cos^2(\theta_e + \theta)}{\cos^2(\theta_e + \theta)}\right\} \tag{19}$$

where

θ is the angle between the normal and the direction of the beam inside the glass

θ_e is the angle between the normal and the direction of the beam outside the glass.

In case the surface is coated, we assume that the reflection coefficient R is a known function of angle and wavelength.

It is well known that there exists a critical angle θ_c such that

$$n \sin\theta_c = 1 \tag{20}$$

Beyond this angle total internal reflection occurs and the reflection coefficient is taken to be unity.

It is desirable to note here that the beams outside of the critial angle which are totally internally reflected arise only through the self-emission within the pane of glass in which they are trapped, while the beams inside the critical angle may also arise because of incident beams or through the self-emission of other panes. This turns out to have an important bearing on the methods employed to calculate the intensities of the two sets of beams, as will be made clear in the section on Numerical Methods, Section III.

In the present treatment, three types of boundary conditions are applicable to the solution of Equation 7. These three types of conditions correspond to three physically different locations. In the first place, there is the glass-air boundary on the outside of the window system. This will always be denoted as boundary #1. Here we let the temperature $T = T_1$ satisfy the condition

$$\left[K \frac{\partial T}{\partial x}\right]_1 + h_1(\bar{T}_1 - T_1) + q_1 - \epsilon_1 \sigma T_1^4 = 0 \tag{21}$$

where

h_1 is the heat transfer coefficient, watts $cm^{-2}(°K)^{-1}$

$\bar{T}_1$ is the temperature of the outside gas, °K

q_1 is the heat absorbed at the boundary, other than by gas conduction or convection, watts cm^{-2}.

The three quantities h_1, $\bar{T}_1$, and q_1 are taken to be prescribed functions of time.

A special word of explanation is needed to describe the surface emissivity ϵ_1 which appears in Equation 21. We must account for the radiation in the opaque wavelength region which is emitted by the surface. We have arbitrarily assumed that this is given by the expression $\epsilon_1 \sigma T_1^4$. This means that ϵ_1 is a function of the temperature T_1 and is given by

$$\epsilon_1(T_1) = \frac{\int_{\lambda_{opaque}} \epsilon(\lambda) B(\lambda, T_1)\, d\lambda}{\sigma T_1^4} \qquad (22)$$

It is to be noted that the radiation in the semitransparent region which crosses the boundary is accounted for separately by the boundary equations on I and J.

In the second place we may treat boundaries which are internal to the system and which face another pane of glass, as shown in Figure 12. Here the boundary condition on T_i is

$$g_j(T_i - T_{i+1}) + \left[K \frac{\partial T}{\partial x}\right]_i + \frac{\alpha_{i+1}\epsilon_i \sigma T_i^4 - \alpha_i \epsilon_{i+1} \sigma T_{i+1}^4}{\alpha_i + \alpha_{i+1} - \alpha_i \alpha_{i+1}} = 0 \qquad (23)$$

where

g_j is the conductance of the intervening gas space, watts $cm^{-2}(°K)^{-1}$

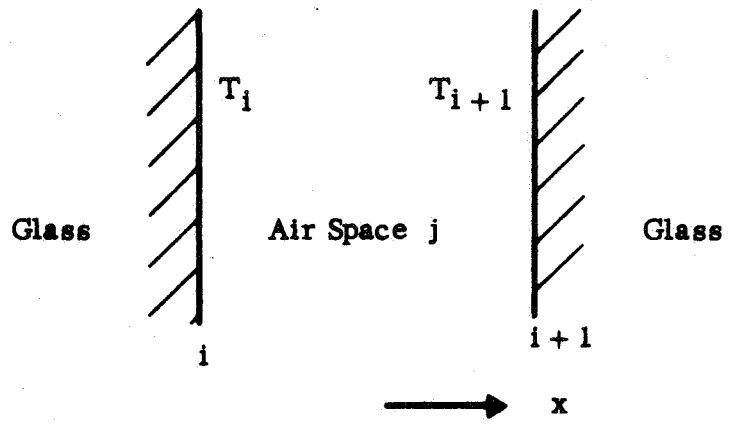

FIGURE 12 BOUNDARIES OF TWO PANES OF GLASS WHICH ENCLOSE AN AIR SPACE

$$\epsilon_i = \frac{\int_{\lambda_{opaque}} \epsilon(\lambda) B(\lambda, T_i)\, d\lambda}{\sigma T_i^4} \tag{24}$$

The quantity α_i is the absorptance of surface i for radiation impinging on it. This radiation is not strictly blackbody, since it arises from surfaces i and i+1 at two different temperatures. It is therefore difficult to give a rigorous definition of α_i. However, if the surface i is grey in the opaque wavelength region, then

$$\alpha_i = \epsilon_i(\lambda_{opaque}) \tag{25}$$

In our work we assume that $\epsilon_i(\lambda_{opaque})$ exists.

In the third place we must treat the final boundary which is on the cabin side of the window system. Here the boundary condition on the temperature T_n is

$$-\left[K \frac{\partial T}{\partial x}\right]_n - \epsilon_n \sigma T_n^4 + g_c(\bar{T}_c - T_n) + \alpha_n \sigma \bar{T}_c^4 = 0 \tag{26}$$

where

T_n is the temperature of the last boundary

$$\epsilon_n = \frac{\int_{\lambda_{opaque}} \epsilon(\lambda) B(\lambda, T_n)\, d\lambda}{\sigma T_n^4} \tag{27}$$

g_c is the heat transfer coefficient from the glass surface to the cabin, watts $cm^{-2}(°K)^{-1}$. This is taken to be constant.

$\bar{T}_c$ is the temperature of the cabin, °K. This is taken to be a prescribed function of the time.

If we assume that the radiation coming from the cabin is blackbody, then

$$\alpha_n = \frac{\int_{\lambda_{opaque}} \epsilon(\lambda) B(\lambda, \bar{T}_c)\, d\lambda}{\sigma \bar{T}_c} \qquad (28)$$

C. INITIAL CONDITIONS

As in all transient thermal problems the initial temperature distribution (say, at time t = 0) must be specified as a function of the coordinate x. It will be observed that the differential Equations 5 and 6 for the beam intensities I and J do not involve any time derivatives and thus these intensities need not be specified initially. Rather, the intensities can be calculated at the initial time by means of the boundary conditions and Equations 5 and 6.

III. NUMERICAL METHODS

A. DIVISION INTO ZONES

In order to solve numerically Equations 5, 6, and 7 with their associated boundary and initial conditions, it is necessary to convert the differential equations into finite difference equations. It is also obviously necessary to restrict to a finite number the values of temperature, time, intensity, angle, and so on to be considered. In doing this we have considered several alternatives and selected the methods which we judge to be the most appropriate.

In the first place, we divide the panes into a number of zones, bounded either by the actual glass-gas interfaces or by imaginary boundaries within the glass. Within each zone we let the temperature vary parabolically as a function of x and we let the intensities of the beams vary exponentially. Each zone is characterized by its mean and boundary temperatures, and the intensities of the beams of radiation crossing the boundaries of the zone. The various pertinent physical properties of the glass which are temperature dependent are evaluated on the basis of the mean temperature of the zone. The exception to this rule is the thermal conductivity K, which is evaluated on the basis of the appropriate boundary temperature. In general, the thermal conductivity will have different values at the two boundaries of the zone.

B. NUMBERING SYSTEMS

A matter which is of crucial importance in developing and describing the algorithms used to solve numerically the heat transport equations is the manner in which the temperatures, beam intensities, spaces, interfaces, and so on which occur in various parts of the system are numbered. In Figure 13, we show an example of a two-pane window system divided into zones. The outer pane is divided into three zones and the inner pane is divided into two zones. In addition to the zones in the glass, the outside air, the space between panes and the cabin are given zone numbers.

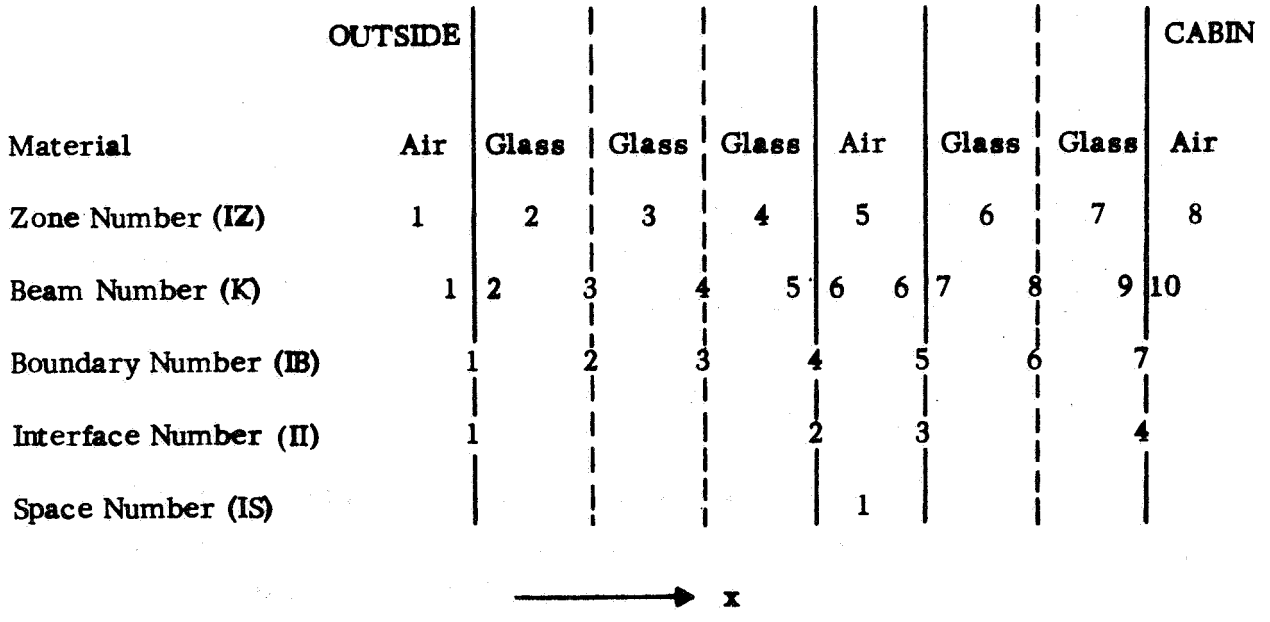

FIGURE 13 **EXAMPLE OF TWO-PANE WINDOW DIVIDED INTO ZONES TO ILLUSTRATE THE NUMBERING SYSTEM USED**

The beam location numbers (K) apply to the beams going in the various directions. It will be observed that beam 1 is just outside the first glass-air interface, beam 2 is just inside the interface, beam 3 is between zones 1 and 2, and so on. Beam 6 is in the space (zone 5) between the panes. Beam 10 is the beam in the cabin, in this example.

It will also be seen that the boundaries are numbered from the outside in, and that each boundary number is equal to the number of the zone to the left of the boundary.

The glass-air interfaces and the gas spaces between panes are also numbered sequentially.

In the following discussion of the numerical methods used to solve the problem, we shall use the example presented in Figure 13 as a model system. The advantage of using a specific example is that we can use integer subscripts on the terms in the equations, while the generalization of the method to other systems will be obvious.

C. APPLICATION OF THE METHOD OF ZONES

We will now describe the extension of the Method of Zones[23] to the solution of the differential Equations 5, 6, and 7. As a first step, however, we will modify Equation 7 slightly. Equations 5 and 6 may be added after multiplying by cosθ to give

$$\cos^2\theta \frac{\partial}{\partial x}(I - J) = \alpha(2E - I - J)\cos\theta \qquad (29)$$

Equation 29 may be integrated with respect to solid angle and wavelength to give

$$\frac{\partial}{\partial x}\iint \cos^2\theta(I - J)\,d\omega d\lambda = \iint \alpha(2E - I - J)\cos\theta\, d\omega d\lambda \qquad (30)$$

Equation 30 may be substituted into the heat balance equation, Equation 7, to give

$$C\rho \frac{\partial T}{\partial t} = \frac{\partial}{\partial x}\left(K \frac{\partial T}{\partial x}\right) - \frac{\partial}{\partial x}\iint \cos^2\theta (I - J)\, d\omega d\lambda \qquad (31)$$

We will use Equations 5, 6, and 31 as the basic differential equations to be solved, subject to suitable boundary and initial conditions.

We may now integrate Equations 5, 6, and 31 with respect to the coordinate x over a typical zone, say zone 2 of Figure 13. We find

$$\cos\theta (I_3 - I_2) = \int_0^{a_2} \alpha (E - I)\, dx \qquad (32)$$

$$\cos\theta (J_2 - J_3) = \int_0^{a_2} \alpha (E - J)\, dx \qquad (33)$$

$$\int_0^{a_2} C\rho \frac{\partial T}{\partial t}\, dx = \left[K \frac{\partial T}{\partial x}\right]_2 - \left[K \frac{\partial T}{\partial x}\right]_1 - \iint \cos^2\theta (I_3 - I_2 + J_2 - J_3)\, d\omega d\lambda \qquad (34)$$

where a_2 is the thickness of the zone.

In order to evaluate approximately the integrals with respect to x which appear in Equations 32, 33, and 34, we let the temperature T(x) in zone 2 have the form

$$T(x) = \bar{T}_2 + \Delta T(x)$$

where $\bar{T}_2 = \frac{1}{a_2}\int_0^{a_2} T(x)\, dx$ is the mean temperature of zone 2, and

$\Delta T(x)$ is the deviation from the mean.

Note particularly that it follows from the definition of $\Delta T(x)$ that

$$\int_0^{a_2} \Delta T(x)\,dx = 0 \tag{35}$$

Now consider a typical integral, say $\int_0^{a_2} \alpha(T)E(T)\,dx$. We may write

$$\alpha(T) = \bar{\alpha}_2 + \frac{\partial \alpha}{\partial T}\,\Delta T + O(\Delta T^2) \tag{36}$$

$$E(T) = \bar{E}_2 + \frac{\partial E}{\partial t}\,\Delta T + O(\Delta T^2) \tag{37}$$

where

$$\bar{\alpha}_2 = \alpha(\bar{T}_2)$$

$$\bar{E}_2 = E(\bar{T}_2)$$

Therefore

$$\int_0^{a_2} \alpha(T)E(T)\,dx = a_2\bar{\alpha}_2\bar{E}_2 + O(\Delta T^2) \tag{38}$$

The terms in ΔT drop out because of Equation 35. In the method of zones we drop the second order term in ΔT^2. In a similar fashion we may evaluate the other integrals in Equations 32, 33, and 34 to obtain

$$\cos\theta(I_3 - I_2) = a_2\bar{\alpha}_2\bar{E}_2 - a_2\bar{\alpha}_2\bar{I} \tag{39}$$

$$\cos\theta(J_2 - J_3) = a_2\bar{\alpha}_2\bar{E}_2 - a_2\bar{\alpha}_2\bar{J} \tag{40}$$

$$a_2\overline{C_2\rho_2}\,\frac{d\bar{T}_2}{dt} = \left[K\,\frac{\partial T}{\partial x}\right]_2 - \left[K\,\frac{\partial T}{\partial x}\right]_1 - \iint \cos^2\theta(I_3 - I_2 + J_2 - J_3)\,d\omega d\lambda \tag{41}$$

where

$$\bar{I} = \frac{1}{a_2}\int_0^{a_2} I(x)\,dx$$

$$\bar{J} = \frac{1}{a_2} \int_0^{a_2} J(x)\,dx$$

$\overline{C_2\rho_2}$ is the heat capacity per unit volume at the mean temperature, $\bar{T}_2$, of the zone.

In the method of zones we assume that the zone is small enough so that, at least for times t of interest, the temperature can be accurately fitted by a parabola in x. To extend the method to account for the radiant interchange, it is necessary to pick some suitable form for the variation of the intensities of the beams. If we consider E and α to be constants, $\bar{E}_2$ and $\bar{\alpha}_2$, respectively, over the zone, it follows from Equations 5 and 6 that

$$I = \bar{E}_2 + Ae^{-\frac{\bar{\alpha}_2 x}{\cos\theta}} \tag{42}$$

$$J = \bar{E}_2 + Be^{\frac{\bar{\alpha}_2 x}{\cos\theta}} \tag{43}$$

where A and B are constants of integration.

The constants of integration, A and B, can be found by using Equations 42 and 43 to find expressions for I_2, I_3, J_2, and J_3 and $\bar{I}$ and $\bar{J}$ and then substituting these expressions into Equations 39 and 40. It is simpler, however, to use the usual methods of differential equations and set x = 0 in Equation 42 and x = a_2 in Equation 43. We find

$$A = I_2 - \bar{E}_2 \tag{44}$$

$$B = (J_3 - \bar{E}_2)e^{-\frac{\bar{\alpha}_2 a_2}{\cos\theta}} \tag{45}$$

Finally, we find

$$I_3 = I_2 e^{-\frac{\bar{\alpha}_2 a_2}{\cos\theta}} + \bar{E}_2\left(1 - e^{-\frac{\bar{\alpha}_2 a_2}{\cos\theta}}\right) \tag{46}$$

$$J_2 = J_3 e^{-\frac{\bar{\alpha}_2 a_2}{\cos\theta}} + \bar{E}_2\left(1 - e^{-\frac{\bar{\alpha}_2 a_2}{\cos\theta}}\right) \tag{47}$$

Equations 46 and 47 are used to calculate the intensities of the emergent beams from zone 2 given the intensities of the incoming beams, the mean temperature, and the physical properties of the glass.

The assumption that T(x) is a quadratic in x within the zone leads to the following formulas for the conductive fluxes across the boundaries:

$$-\left[K\frac{\partial T}{\partial x}\right]_1 = -\frac{K_1}{a_2}(6\bar{T}_2 - 4T_1 - 2T_2) \tag{48}$$

$$\left[K\frac{\partial T}{\partial x}\right]_2 = -\frac{K_2}{a_2}(6\bar{T}_2 - 4T_2 - 2T_1) \tag{49}$$

where

T_1 and T_2 are the boundary temperatures
K_1 and K_2 are the thermal conductivities at the boundaries

Now we may substitute Equations 46, 47, 48, and 49 into Equation 41 to obtain

$$a_2\overline{C_2\rho}_2\frac{d\bar{T}_2}{dt} = -\frac{K_2}{a_2}(6\bar{T}_2 - 4T_2 - 2T_1) - \frac{K_1}{a_2}(6\bar{T}_2 - 4T_1 - 2T_2)$$

$$+\iiint\left(1 - e^{-\frac{\bar{\alpha}_2 a_2}{\cos\theta}}\right)(I_2 + J_3 - 2\bar{E}_2)\cos^2\theta\, d\omega d\lambda \tag{50}$$

In Equation 50 the indicated integrations must be performed numerically. We use the trapezoidal rule to integrate with respect to λ over the semitransparent part of the spectrum. We use a weighted sum to integrate over the solid angle.

D. SOLUTION OF EQUATIONS FOR MEAN TEMPERATURES

It will be seen that Equation 50 is an ordinary first order differential equation. In the typical example depicted in Figure 13, five such equations (for $\overline{T}_2$, $\overline{T}_3$, $\overline{T}_4$, $\overline{T}_6$, and $\overline{T}_7$) would have to be set up and solved. The differential equations are solved by the standard fourth order Runge-Kutta method.

We find that the use of an explicit method, rather than an implicit method, is advantageous in the present case. The main reason is that the large number of beam equations are "decoupled" into small groups to be solved simultaneously. The disadvantage of the explicit method, namely, the possibility of instability if too large a time interval is used, can be safely ignored since the thermal masses of the various zones will be approximately the same so that the time step appropriate to one zone will be more or less appropriate to all the zones. A rough calculation indicates that if the zone is a few millimeters thick, a time step of the order of one second will not cause instability.

Clearly, the initial conditions for solving the differential equations of the type of Equation 50 are the initial values of the mean temperatures of the glass zones. All other quantities must be either computed or prescribed as boundary conditions.

E. METHODS OF SOLVING FOR THE BEAM INTENSITIES

The beams fall into two groups, according to whether the angle

between the direction of the beam and the normal (x-coordinate) is less than or greater than the critical angle. If the angle is less than the critical angle, the beam is a penetrating beam that traverses through all the panes. If the angle is greater than the critical angle, the beam is a totally internally reflected beam and is confined to a single pane. The equations governing the intensities of the two groups of beams are quite similar, but the methods for solving the equations are quite different. We solve the equations for the intensities of the penetrating beams by iteration and the equations for the intensities of the totally internally reflected beams by substitution.

In order to demonstrate the methods, we consider the example shown in Figure 13. First of all we will write down the typical equations which govern the intensities of the penetrating beams at one angle and wavelength.

$$I_1 = \text{given} \tag{51.1}$$

$$I_2 = n^2(1 - R_1)I_1 + R_1 J_2 \tag{51.2}$$

$$I_3 = \eta_2 I_2 + W_2 \tag{51.3}$$

$$I_4 = \eta_3 I_3 + W_3 \tag{51.4}$$

$$I_5 = \eta_4 I_4 + W_4 \tag{51.5}$$

$$I_6 = \frac{1}{n^2}(1 - R_2)I_5 + R_2 J_6 \tag{51.6}$$

$$I_7 = n^2(1 - R_3)I_6 + R_3 J_7 \tag{51.7}$$

$$I_8 = \eta_6 I_7 + W_6 \tag{51.8}$$

$$I_9 = \eta_7 I_8 + W_7 \tag{51.9}$$

$$I_{10} = \frac{1}{n^2}(1 - R_4)I_9 + R_4 J_{10} \tag{51.10}$$

$$J_{10} = \text{given} \tag{51.11}$$

$$J_9 = n^2(1 - R_4)J_{10} + R_4 I_9 \tag{51.12}$$

$$J_8 = \eta_7 J_9 + W_7 \tag{51.13}$$

$$J_7 = \eta_6 J_8 + W_6 \tag{51.14}$$

$$J_6 = \frac{1}{n^2}(1 - R_3)J_7 + R_3 I_6 \tag{51.15}$$

$$J_5 = n^2(1 - R_2)J_6 + R_2 I_5 \tag{51.16}$$

$$J_4 = \eta_4 J_5 + W_4 \tag{51.17}$$

$$J_3 = \eta_3 J_4 + W_3 \tag{51.18}$$

$$J_2 = \eta_2 J_3 + W_2 \tag{51.19}$$

$$J_1 = \frac{1}{n^2}(1 - R_1)J_2 + R_1 I_1 \tag{51.20}$$

where

$$\eta_2 = e^{-\frac{\bar{\alpha}_2 a_2}{\cos\theta}}, \text{ etc.}$$

$$W_2 = \bar{E}_2\left(1 - e^{-\frac{\bar{\alpha}_2 a_2}{\cos\theta}}\right), \text{ etc.}$$

R_1 is the reflection coefficient at interface 1, etc.

Equations 51 may be solved by setting all intensities (except I_1 and J_{10}) equal to zero (or some other approximation to the final values) and then successively improving the approximations by calculating I_2 from Equation 51.2, I_3 from Equation 51.3, and so on through all the equations iteratively until the equations are all satisfied to the desired accuracy. Note that beams at different angles and wave-

lengths do not interact with each other in this part of the process, so that the large number of beam equations is broken down into many relatively small groups and an iterative process involving many hundreds or even thousands of coupled equations is avoided.

In the case of the totally internally reflected beams matters are even simpler. We will write the equations for the intensities of the beams traversing zones 6 and 7 as shown in Figure 13. We find

$$I_7 = J_7 \tag{52.1}$$
$$I_8 = \eta_6 I_7 + W_6 \tag{52.2}$$
$$I_9 = \eta_7 I_8 + W_7 \tag{52.3}$$
$$J_9 = I_9 \tag{52.4}$$
$$J_8 = \eta_7 J_9 + W_7 \tag{52.5}$$
$$J_7 = \eta_6 J_8 + W_6 \tag{52.6}$$

These equations have a particularly simple form, which enables us to obtain the solution for I_7 by a sequence of substitutions. We may write

$$I_7 = \frac{W_6 + \eta_6(W_7 + \eta_7(W_7 + \eta_7 W_6))}{1 - \eta_6^2 \eta_7^2} \tag{53}$$

The rest of the unknowns may be found by successive numerical substitutions in Equations 52.

Just to make clear the generalization of Equation 53, we will also exhibit the solution for the intensity I_2 in the outer pane:

$$I_2 = \frac{W_2 + \eta_2(W_3 + \eta_3(W_4 + \eta_4(W_4 + \eta_4(W_3 + \eta_3 W_2))))}{1 - \eta_2^2 \eta_3^2 \eta_4^2} \tag{54}$$

Note that in the numerator all the W_i are used twice, in forward and reverse order, and all of the η_i except the one with the smallest subscript are used twice.

F. CALCULATION OF BOUNDARY TEMPERATURES

In this section we shall show how to set up the equations needed to determine the boundary temperatures. The boundaries that we must consider are of two types, namely, real boundaries at glass-gas interfaces and fictive zone boundaries which are introduced by dividing the panes into zones. We have discussed the conditions which are theoretically to be met at the real boundaries. At the fictive boundaries, the requirements are simply that temperature and conductive flux be continuous. The continuity of temperature is assured by the numbering system used. The requirement for continuity of thermal flux provides us with an equation from which the boundary temperature can be calculated. For example, at boundary 2, we may write

$$K\left[\frac{\partial T}{\partial x}\right]_{2-} = K\left[\frac{\partial T}{\partial x}\right]_{2+} \tag{55}$$

Here 2- and 2+ are used to indicate the positions just to the left and right of the boundary, respectively.

In order to solve the boundary equations numerically, it is necessary to replace the partial derivatives with respect to x by the appropriate formulas of the types given in Equations 48 and 49.

At boundary 1, Equation 21 is replaced by the equation

$$\frac{K_1}{a_1}(6\bar{T}_2 - 4T_1 - 2T_2) + h_1(\bar{T}_1 - T_1) + q_1 - \epsilon_1\sigma T_1^4 = 0 \tag{56}$$

This equation is not really a quartic in T_1, since ϵ_1 and K_1 are functions of T_1. It may be solved as a quartic, however, as though ϵ_1 and K_1 were known, and then solved again with adjusted values of K_1 and ϵ_1 until the equation is satisfied to the desired accuracy. This method of solving the pseudo-quartic equation for the first boundary tempera-

ture may be used for solving all the pseudo-quartic equations which determine the temperatures at the other real boundaries.

Boundary 2 is a fictive boundary. Here Equation 55 is replaced by the equation

$$\frac{K_2}{a_2}(6\bar{T}_2 - 4T_2 - 2T_1) + \frac{K_2}{a_3}(6\bar{T}_3 - 4T_2 - 2T_3) = 0 \qquad (57)$$

In this case the conductivity K_2 may be divided out and the equation can be solved explicitly for T_2

$$T_2 = \frac{(3\bar{T}_2 - T_1)a_3 + (3\bar{T}_3 - T_3)a_2}{2(a_2 + a_3)} \qquad (58)$$

Formulas for all fictive boundary temperatures can be similarly written.

$$T_3 = \frac{(3\bar{T}_3 - T_2)a_4 + 3(\bar{T}_4 - T_4)a_3}{2(a_3 + a_4)} \qquad (59)$$

$$T_6 = \frac{(3\bar{T}_6 - T_5)a_7 + 3(\bar{T}_7 - T_7)a_6}{2(a_6 + a_7)} \qquad (60)$$

The equation which governs T_4, the temperature of the interface at the left of the air space is derived from Equation 23.

$$g_1(T_4 - T_5) - \frac{K_4}{a_4}(6\bar{T}_4 - 4T_4 - 2T_3) + \frac{\alpha_5\epsilon_4\sigma T_4^{\,4} - \alpha_4\epsilon_5\sigma T_5^{\,4}}{\alpha_4 + \alpha_5 - \alpha_4\alpha_5} = 0 \qquad (61)$$

A similar equation determines the temperature T_5 of the interface at the right of the air space.

$$g_1(T_4 - T_5) + \frac{K_5}{a_6}(6\bar{T}_6 - 4T_5 - 2T_6) + \frac{\alpha_5\epsilon_4\sigma T_4^{\,4} - \alpha_4\epsilon_5\sigma T_5^{\,4}}{\alpha_4 + \alpha_5 - \alpha_4\alpha_5} = 0 \qquad (62)$$

The definition of α_4 and α_5 is given by Equation 25.

The final boundary temperature equation to be discussed is the equation for T_7. This equation is derived from Equation 26 and is

$$\frac{K_7}{a_7}(6\bar{T}_7 - 4T_7 - 2T_6) - \epsilon_7\sigma T_7^4 + g_c(\bar{T}_8 - T_7) + \alpha_7\sigma\bar{T}_8^4 = 0 \qquad (63)$$

Note that the definition of α_7 is given by Equation 28.

We have explained how the individual equations may be solved, either explicitly or by iteration. The set of equations to determine the boundary temperatures must be solved simultaneously. This is also accomplished by iteratively solving the set of equations one by one, again and again, until the set is satisfied to sufficient accuracy.

G. THE ENERGY BALANCE

As a general check on the calculation of the temperatures and beam intensities, an overall energy balance is made at each step. We calculate the total energy, E_{in}, that has entered the system, the total energy, E_{out}, that has left the system, the energy, E_0, stored in the system at time t = 0, and the present energy, E_p, that is stored in the system at time t. Then the disparity, E_s, in the energy balance is calculated from the equation

$$E_s = E_p - E_0 - E_{in} + E_{out} \qquad (64)$$

The trapezoidal rule is used to integrate the input flux, q_{in}, and the output flux, q_{out}, with respect to time to obtain the energies E_{in} and E_{out}, respectively. The input and output fluxes may easily be determined from consideration of the boundary conditions. We find (again we refer to the example shown in Figure 3) that

$$q_{in} = \iint I_1\cos\theta\, d\omega\, d\lambda + h_1\bar{T}_1 + q_1 + \iint J_{10}\cos\theta\, d\omega d\lambda + g_c\bar{T}_8 + \alpha_7\sigma\bar{T}_8^4 \qquad (65)$$

$$q_{out} = \iint J_1\cos\theta\, d\omega\, d\lambda + h_1T_1 + \epsilon_1\sigma T_1^4 + \iint I_{10}\cos\theta\, d\omega\, d\lambda + g_cT_7 + \epsilon_7\sigma T_7^4 \qquad (66)$$

By the trapezoidal rule

$$E_{in}(t + \Delta t) = E_{in}(t) + \frac{\Delta t}{2}\left[q_{in}(t) + q_{in}(t + \Delta t)\right] \tag{67}$$

$$E_{out}(t + \Delta t) = E_{out}(t) + \frac{\Delta t}{2}\left[q_{out}(t) + q_{out}(t + \Delta t)\right] \tag{68}$$

The total stored energy of the system at any time is obtained by adding up the energies stored in the individual zones. The energy stored in a zone, say zone 2, is given by the integral

$$E_{p2} = \rho_2 a_2 \int_0^{\overline{T}_2} C_2(T)\,dT \tag{69}$$

If the heat capacity is given as a polynomial function of the temperature, the integration is easily carried out.

H. SUMMARY OF THE METHOD

In the preceding sections we have shown how the various unknowns may be approximately calculated. In this summary we will give a brief description of how all the methods described are brought together to form the complete algorithm for solving the present heat transport problem.

We assume that all the necessary system boundary values are properly prescribed at all times.

At time t = 0 the mean temperatures of all the zones are given. Since the mean temperatures are known, the intensities of penetrating beams and the totally internally reflected beams can be calculated. So also, all boundary temperatures can be computed. Thus the state of the system is completely known at the initial instant. This, in turn, enables us to calculate the time derivatives of the mean temperatures of the zones, so that the mean temperatures may be extrapolated. As soon

as this is done the cycle is complete, and new values of the beam intensities and boundary temperatures can be computed.

As the time is advanced, the energy balance check is made, and at selected time intervals the discrepancy in the energy balance may be observed and compared with the total incoming energy and the stored energy to see if any substantial error in the results is being built up.

PART 3

EXPERIMENTAL PROGRAM

I. INTRODUCTION AND SUMMARY

The purpose of the experimental phase of this program was to examine experimentally the validity of the computer program developed in an earlier phase. An apparatus was set up in which to give test windows transient exposure to high temperature radiation while at the same time the temperatures of the two window faces and the radiant power passing through the windows were measured. The apparatus worked properly and produced results in substantial agreement with those predicted by the computer for the same experimental conditions.

Quartz and aluminosilicate window samples were exposed by being placed suddenly at a fixed position near a source of blackbody radiation in vacuum and kept there for a period of 300 seconds. The highest source temperature in these tests was 1300°K which resulted in an incident irradiance delivered at the test window of the order of 7 watts/cm^2 and final window temperature after 300 seconds of the order of 800°K. Somewhat more than half of the irradiance delivered to the windows was transmitted directly through the window, the remaining irradiance being absorbed and eventually re-radiated by the body of the window.

Tests were performed also on a reflective gold-film coated quartz window for the purpose of simulating heat reflecting windows. However, results of these tests were not significant because the gold films proved not to be thermally stable. Because of thermal destruction, the film coated sample did not differ significantly in its thermal behavior from clear quartz. Reflectance measurements made subsequent to the thermal tests showed that the film coated quartz window did not exhibit significant infrared reflectance.

The test windows for all tests were 6.35 cm diameter, 0.635 cm thick disks on each side of which was deposited a very thin and non-

obstructing grid of gold film for the purpose of resistive thermometry of the two window surfaces. Total irradiance through the window was measured with a total radiation radiometer brought very close to the back face of the window.

II. APPARATUS AND METHOD

A. SUMMARY DESCRIPTION

The heart of the apparatus for exposing and measuring windows is shown in Figures 14 through 17. A blackbody cavity is mounted just below a water cooled aperture plate that defines accurately an area radiating to the test window above the cavity. The cavity and aperture plate are stationary. Above the cavity is a water cooled rotatable sample wheel with four positions in one of which is mounted the test window in a thermally insulating holder. During a test, the wheel is rotated to bring the cool window from a room temperature environment away from the cavity to a position directly above the cavity. The other three positions of the sample wheel are occupied by a dummy window and two open holes. A Gardon-type foil radiometer is slide mounted on the axis of cavity and window, so that it can be positioned and locked at any chosen distance from the back of the test window or at any chosen distance from the cavity when the sample wheel is in an open hole position. The cavity and cavity element, sample and sample wheel, radiometer, and associated equipment are operated in a vacuum chamber comprised of a water cooled stainless steel bell jar evacuated by an oil diffusion pumping system. The sample wheel may be rotated and the radiometer moved while the system is evacuated and while the cavity is hot. Tests are observed in progress through a 17.8 cm diameter Vycor window through which cavity temperatures are measured with an optical pyrometer.

The 45.7 cm diameter vacuum bell jar housing and the fixtures inside it are all water cooled and painted black to present a uniform and well defined ambient irradiance to the test window.

The sample gold film temperature sensing grids were calibrated before a test. That is, the electrical resistivity of grid elements as a function of temperature was measured. This calibration was carried out

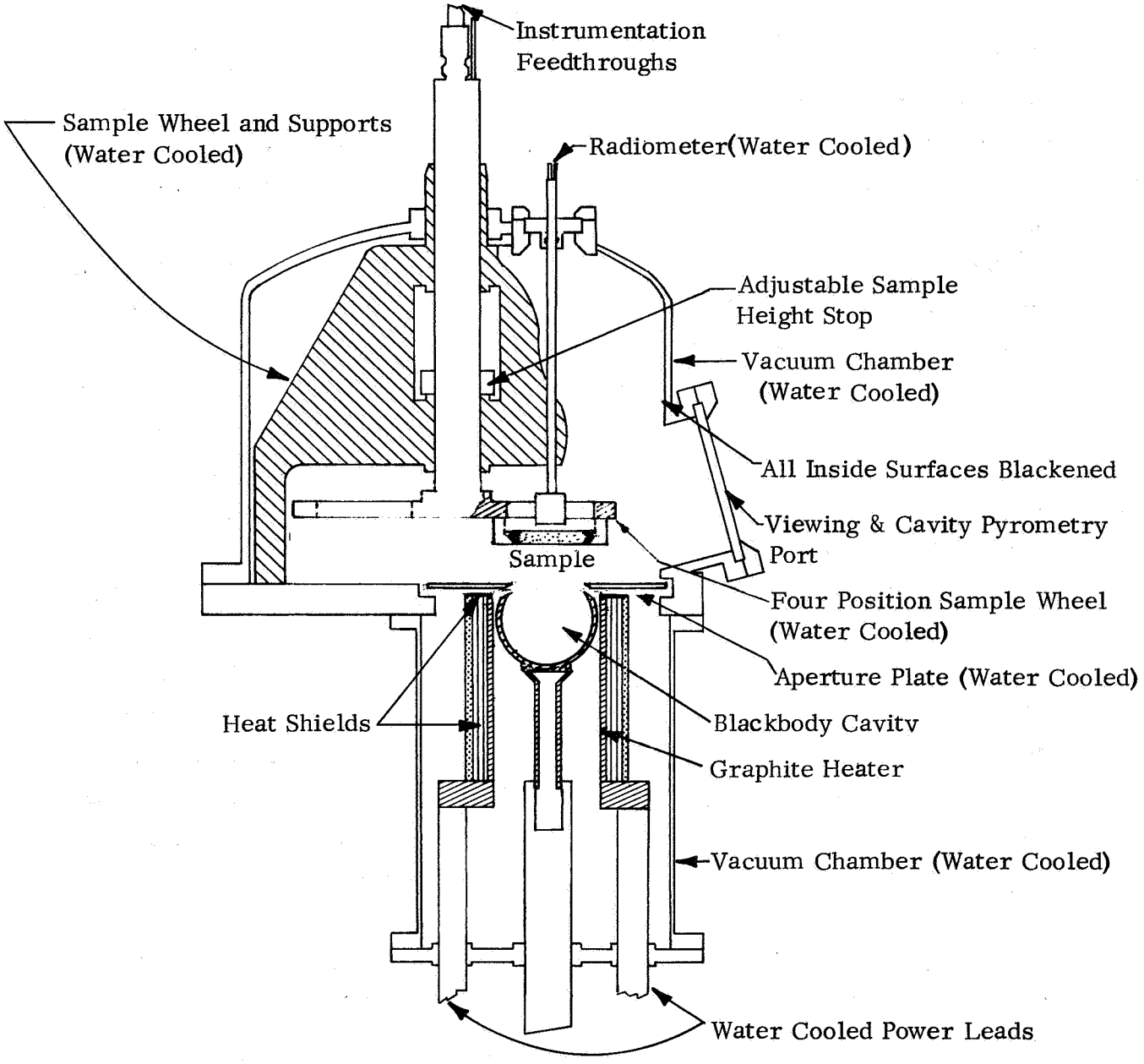

FIGURE 14 TEST APPARATUS

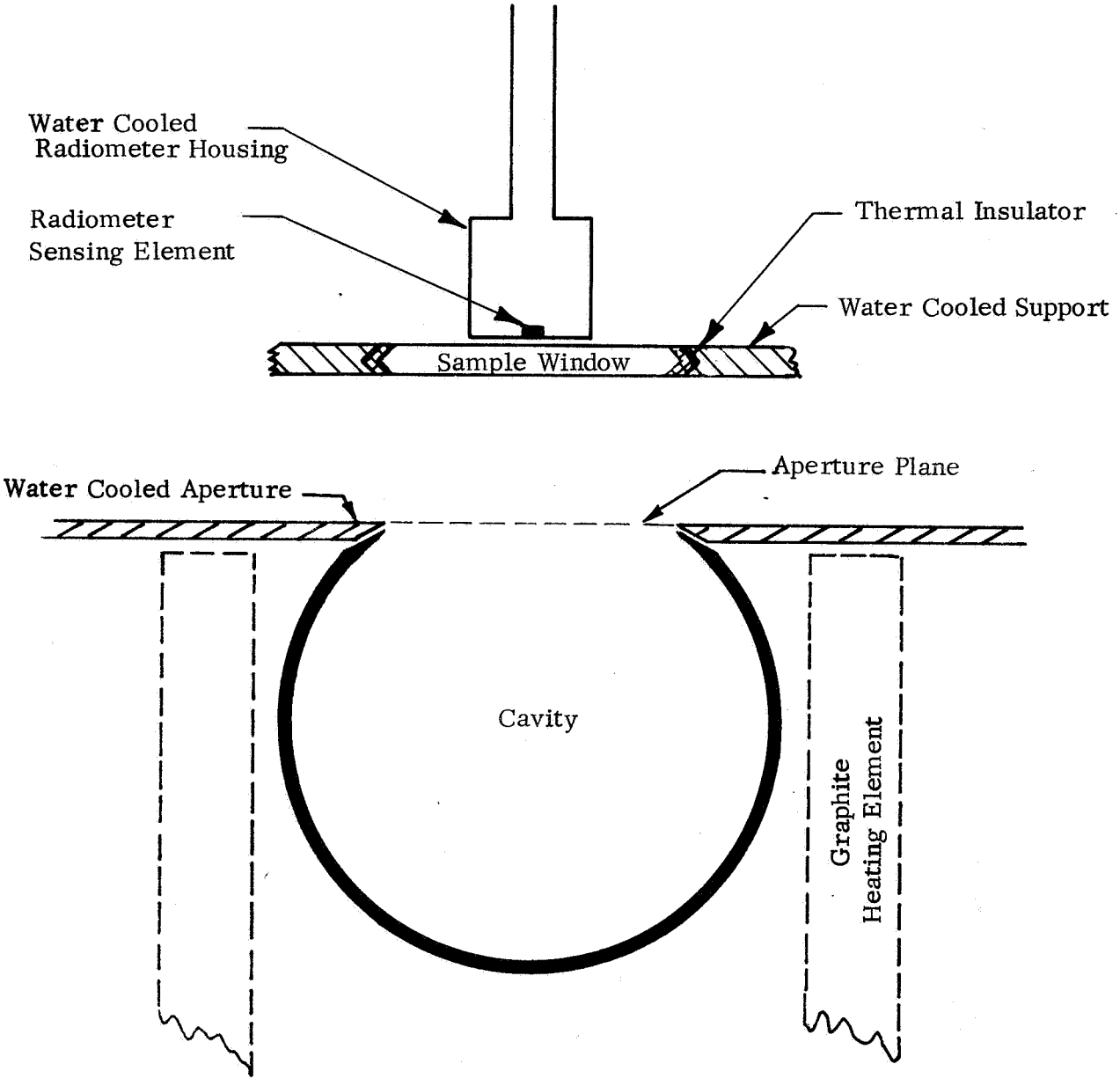

FIGURE 15 TEST GEOMETRY

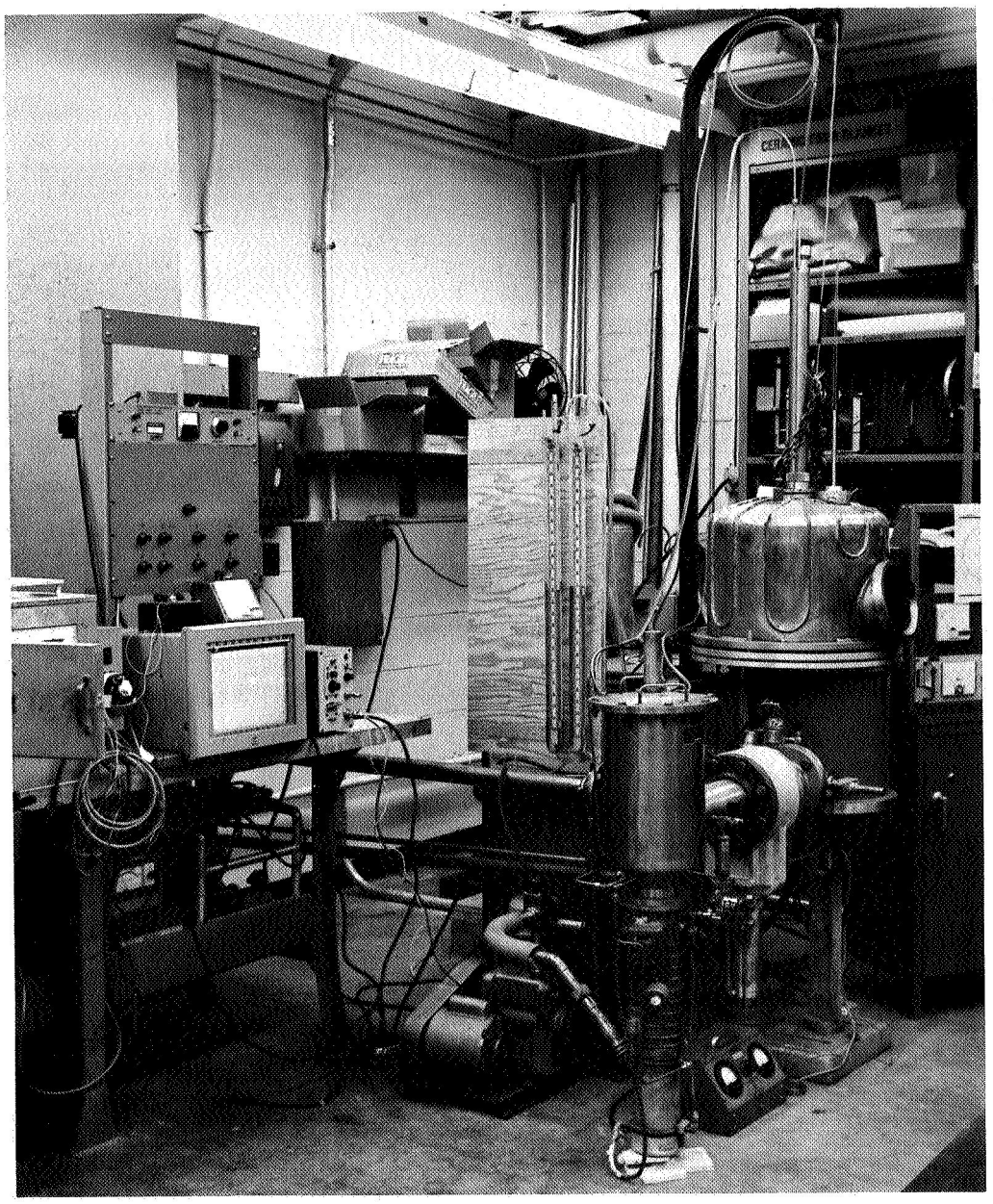

FIGURE 16 PHOTOGRAPHIC VIEW OF TEST SET-UP

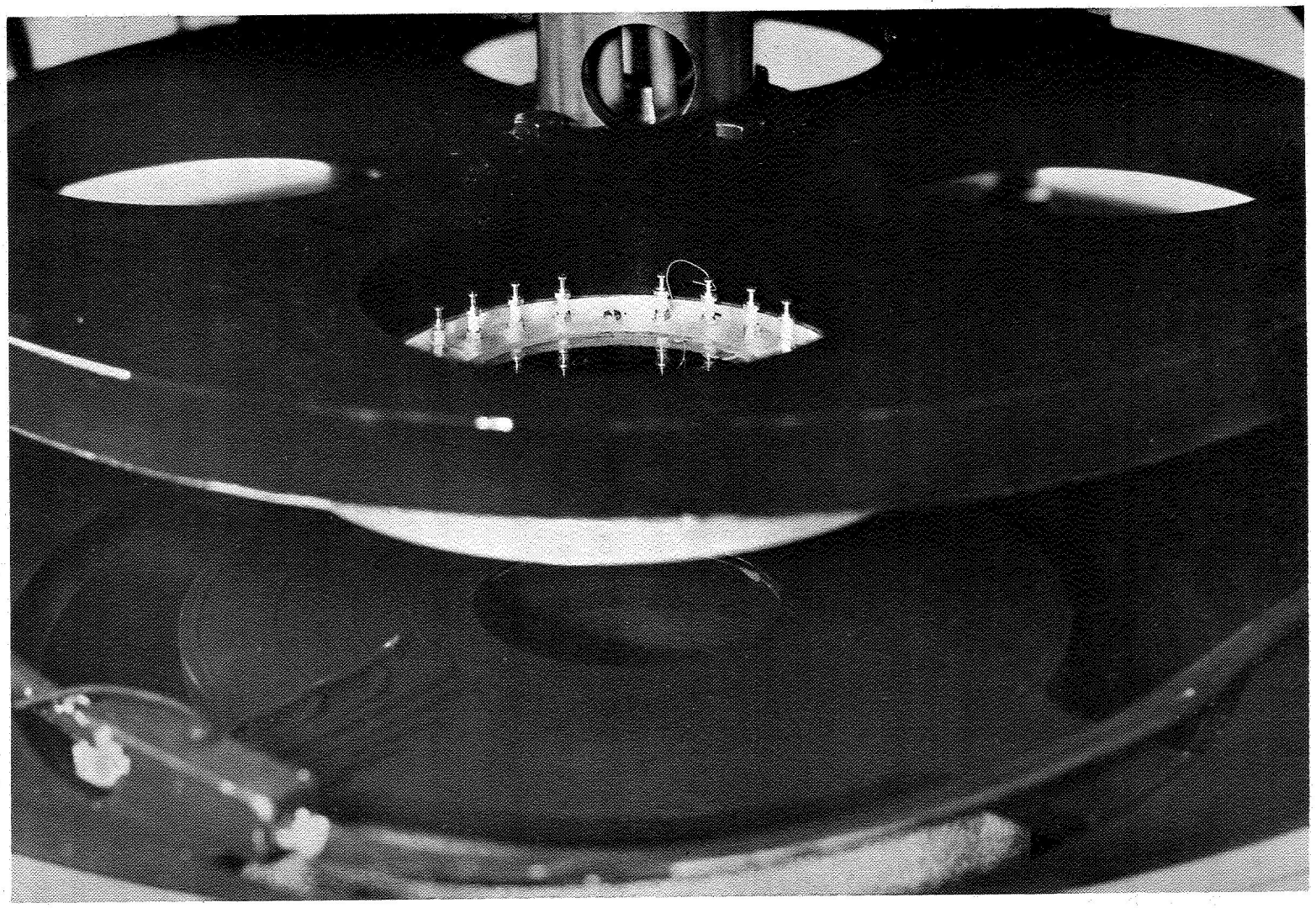

FIGURE 17 PHOTOGRAPHIC VIEW SHOWING TEST ARRANGEMENT OF CAVITY SOURCE AND TEST WINDOW

in a separate air filled oven in which the sample and an accurate thermocouple placed near it are both allowed to come to the same equilibrium temperature in the oven. This calibration procedure was repeated for several different temperatures covering the range of temperatures expected during actual test.

During any given test, temperature and irradiance data were recorded continuously on multi-channel recorders. Outputs from the gold grid temperature sensors on the window test samples and from the radiometer behind the windows were recorded simultaneously on the same strip chart.

B. WINDOW HEAT SOURCE

1. Cavity Design

The blackbody cavity source was critical to an accurate irradiance experiment. A spherical cavity was selected because of its rather uniquely useful properties as discussed by Sparrow and Jonsson.[22]

A spherical cavity with a Lambertian wall delivers equal irradiance from any one element on its surface to any other element on its surface. As a consequence of this property, each area element of its inside wall will contribute equally to the radiant power flowing out of a diminishing small aperture cut in it. A second consequence of this property is that such a cavity having uniform wall thickness, if fed heat from a heat source from outside, will have an isothermal inner surface. Thus, the radiation from a small aperture in a sphere is closely represented by a single Planck function, not a distribution of Planck functions due to temperature gradients necessary for equilibrium heat distributions in other cavity shapes. If the size of the aperture in the sphere is increased in respect to its radius, and if the walls are only approximately Lambertian, the spherical cavity is still more nearly isothermal of equivalent volume, open area, and wall thickness

The cavity used as a blackbody source in our experiment was machined from ATJ graphite, had an inside diameter of 9.52 cm, a wall thickness of 0.317 cm and an aperture opening the same diameter as the test windows to be irradiated, 6.35 cm. The subtended half angle of the aperture from the center of the spherical cavity was 45 degrees.

The cavity was machined with a tapered feather edged lip at the aperture which mated to a corresponding feather edged taper in the water cooled aperture plate. The aperture plate was spaced very close to but not touching the cavity lip. The cavity was supported from below by a graphite pedestal. Temperature expansion in this pedestal and other structure cause the spacing between cavity and aperture plate to vary slightly but this effect was negligible. The design thus approached closely the ideal of a geometric planar slice off the side of the heated cavity exposing no more and no less than the circular hole in the sphere as a source to irradiate the test window.

The underside of the water cooled aperture plate is gold plated and polished to achieve an estimated total hemispherical reflectance of .97 to radiation at the cavity temperature used, the purpose being to minimize radiant transfer from cavity to plate. Also, tantalum heat shields are used to minimize losses in the desired heat transfer from heating element to cavity.

The cavity was heated by a cylindrical graphite heating element surrounding the cavity sphere. The element is 10.9 cm inside diameter, 20 cm long, and is resistively heated by a 60 cycle, single phase AC source. The element is capable of liberating up to 16 kilowatts of thermal power. The element is surrounded by two tantalum and one vitreous quartz heat shields. The surrounding vacuum housing is water cooled and blackened on the inside, contains water cooled power feedthroughs and a 7.6 cm diameter connection to the external vacuum pumping and gauging system. The furnace unit, heating element, shields, housing,

and power supply were purchased as standard components of a commercially available crystal pulling furnace,* and then modified by us as necessary.

The furnace was controlled by a saturable core reactor which is included as part of the NRC power supply. The saturable core reactor, in turn, was controlled by DC current from a precision regulated and adjustable DC supply. The heating power was controlled manually, the operation monitored by an AC ammeter and voltmeter connected into the heating element power circuit. One power setting without further adjustment proved sufficient for maintaining an accurate cavity temperature during a window exposure test.

2. Cavity Temperature Measurement

The temperature of the cavity during a window exposure test was measured using a standard laboratory pyrometer** operating in the visible red, the reading then being corrected for the effects of the spectral emittance of the cavity and for the effects of the intervening Vycor vacuum chamber window. Fortunately, the effects on cavity temperature measurements of uncertainties in spectral emittance were very slight at the source temperatures used in tests.

The computation and corrections for pyrometer error are detailed in Appendix A. The corrections required in these experiments due to cavity emittance and a fresnel reflection loss at each face of a Vycor observation window amounted to 7°K at the 1300°K cavity operating temperature and 5°K at the 1125°K operating temperature.

The pyrometer used in these experiments was checked within three weeks of all experiments against a new General Electric tertiary

---

* Model 2805, Product of National Research Corporation (NRC), Needham, Massachusetts.

** Product of Pyrometer Instrument Company, Bergenfield, New Jersey.

tungsten optical standard lamp. The pyrometer readings were repeatable within ± 1.7°K with a precision of ± 5°K.

3. Cavity Temperature Variations

Two variations in cavity temperature are of interest during a test: variations with time and spatial variations across the emitting aperture of the cavity.

The time variations of cavity temperature are small due to the fact that the thermal time constants of the cavity heating element and cavity are long compared to the duration of a 300 second window exposure test and due also to the fact that the power to the heating element is steady.

Time variations in cavity temperature were measured. It was found with one power setting to the heating element that the cavity temperature varied within ± 2°K for all tests and typically varied less than ± 1°K of the average value after cavity equilibrium conditions had been reached. The greatest variation within these limits occurred when a window reached a high enough temperature to begin radiating appreciably back into the cavity leading to a rise in cavity temperature of 1°K.

Spatial variations of temperature across the cavity aperture are related to gradients in the cavity wall and also to unequal radiant power distributions within the cavity due to the presence of a finite aperture. These variations were expected to be small on the basis of the design. Measurements confirmed these expectations. The cavity at an equilibrium temperature typical of the test was scanned across its aperture with an optical pyrometer focused on the plane of the aperture, from a normal and oblique angle. Fifteen regions on the aperture were measured. The cavity at an average temperature of 1293°K was found to fall at all points within a 14°K range; the standard deviation being 4°K.

In summary the variation among the various cavity temperature readings were of the order of 1/2 percent of absolute temperature. Corresponding to these temperature variations were radiance variations of 2 percent.

4. Cavity Emittance

Ideally a blackbody source should have an emittance equal to one at all angles, wavelengths, and temperatures. Within practical constraints, one designs for an emittance approaching the ideal.

The balance between conflicting considerations effecting the cavity design, such as the desire for a large aperture diameter and a large cavity diameter to aperture diameter ratio, and the need for maintaining reasonable limits on cavity heater power requirements and equipment costs led to the cavity design previously discussed.

The determination of the emittance, ε_a, of the resulting cavity was obtained by calculation, using Sparrow's[22]a expression for the total hemispherical emittance of a spherical cavity with a large aperture:

$$\varepsilon_a = \frac{\varepsilon}{\left[1 - .5\ (1-\alpha)(1+\cos\ \phi)\right]} \tag{70}$$

where

ε_a = the total hemispherical emittance of the cavity as seen at the aperture.

ε = the total hemispherical emittance of the wall material of the cavity.

α = the total hemispherical absorptance of the wall material of the cavity.

ϕ = the half angle subtended by the aperture at the center of the spherical cavity.

The application of this equation requires that the total

absorptance of the cavity wall equals the total emittance of the wall, i.e., $\varepsilon = \alpha$. This latter constraint is closely met under the special conditions existing inside a good cavity; that is, where the incident radiation at each point on the wall arises from a source (the rest of the cavity) at very nearly the same temperature at which heat is radiated from the wall element under consideration.

The half angle subtended by a circular aperture in a sphere is fixed as a consequence of the geometry of the sphere when together the aperture diameter and sphere inside diameters are fixed. For the cavity used in these experiments the aperture diameter of 6.35 cm and sphere inside diameter of 10.9 cm fix the half angle at $\phi = 45.0°$. Inserting the foregoing conditions into equation (70), calculations were made with the results shown in Figure 18.

A value for total emittance of the graphite cavity wall is required in order to calculate cavity emittance. However, the wall emittance need not be determined accurately in view of the fact that aperture emittance is relatively insensitive to wall emittance. For the range of operating conditions for this cavity, a 6 percent error in wall emittance generates a 1 percent error in cavity emittance as seen at the aperture.

The wall emittance of our cavity was estimated on the basis of the data of Plunkett and Kingery[19] for ATJ graphite and using their empirical equations that quantify the necessary corrections for temperature of the graphite surface and its grit roughness. The inside surface of our cavity was estimated to have a roughness corresponding to 150 grit and an estimated total emittance of 0.72 in the temperature range of use 1125°K to 1300°K.

The range within which the true wall emittance value was likely to fall with respect to the assumed value also was estimated. Based on

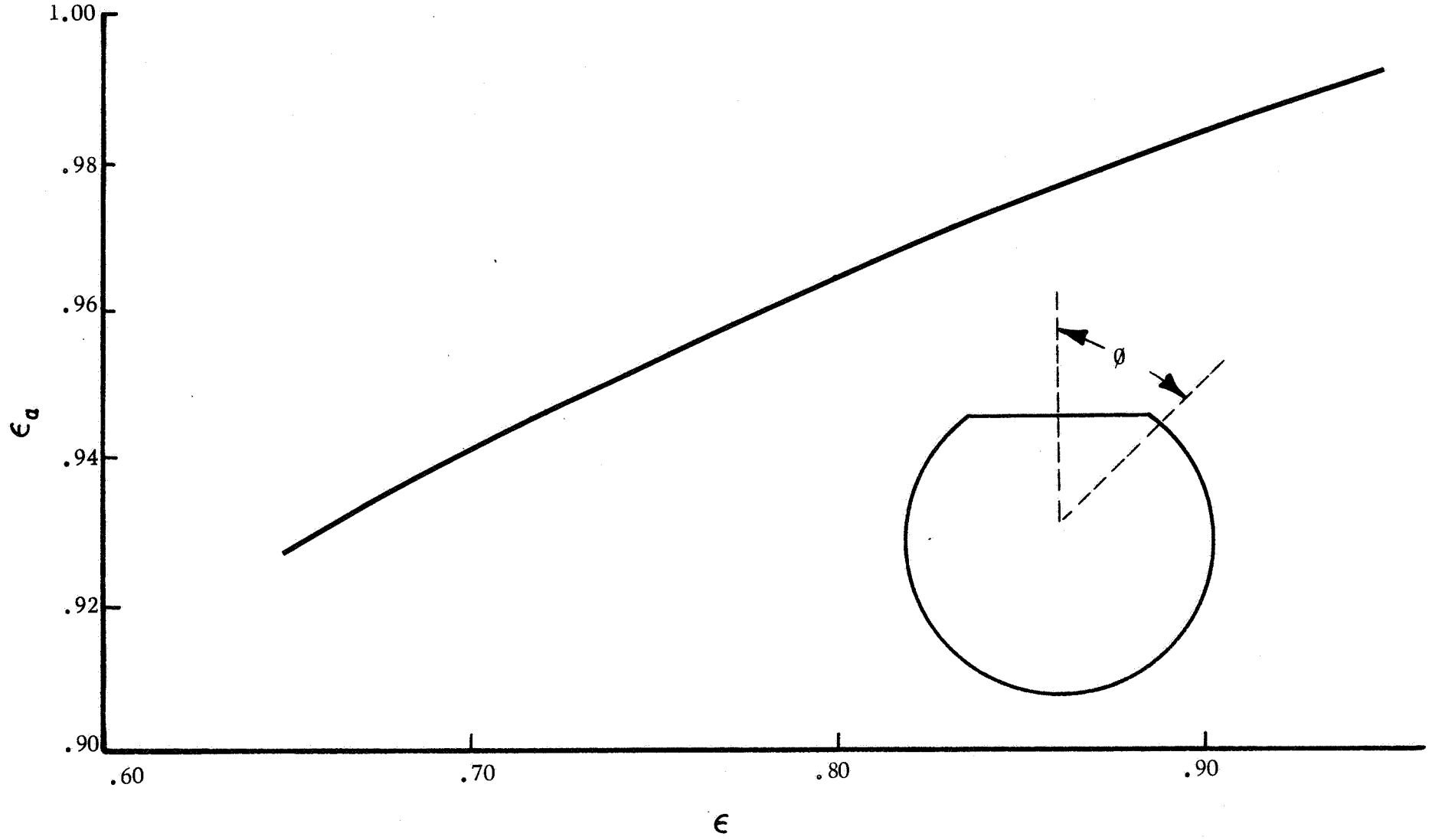

FIGURE 18 EFFECTIVE EMITTANCE OF A SPHERICAL CAVITY OF ø = 45° OPENING VS WALL EMITTANCE

Plunkett and Kingery's data and taking into account differences between the two ends of the cavity temperature range and errors in our estimate of graphite roughness, the error in wall emittance is small, of the order of 3 percent and the resulting cavity emittance error of the order of 1/2 percent. However, in view of the broader scatter of graphite emittance data reported in the literature, it appeared reasonable to assign an error of the order of $\pm$ 15 to $\pm$ 20 percent to our estimate of wall emittance. The corresponding estimate of cavity emittance error is 1/6 of this, or $\varepsilon_a = .95 \pm .03$.

A mean value of 0.95 was used for data reduction purposes in all experiments although they involved cone angles smaller than hemispherical (e.g., 40° half angle) and two cavity temperature levels, 1300°K and 1125°K. By implication the spectral emittance was also assumed to be approximately equal to the above value within the cavity wavelength range of interest, 1.3 microns to 13 microns.

C. TEST WINDOWS

1. Thermophysical Data

Technical information provided by the Technical Products Division of the Corning Glass Works was the primary source of thermophysical property data inserted as input to computer simulations and used, as required, in the design of experiments and the interpretation of results. In large measure, this data was extracted from published Technical Information Bulletins by the Corning Glass Works on:

1. fused silica glass, Corning Code No. 7940, copyright 1965;
2. aluminosilicate glass, Corning Code No. 1723, copyright 1963;
3. 96 percent silica glass, Corning Code No. 7913, copyright 1964.

For reference data on the transmission and reflective properties of gold films, technical data provided by Libbey-Owens-Ford Glass Company

was consulted. The spectral transmission and reflective properties of the gold films inserted into our computer simulations of tests involving gold film coated glass samples were based on this data.

Data on refractive index, density, and on thermal conductivity and specific heat as a function of temperature were taken directly from the Corning publications. The spectral absorption coefficient α_λ was computed by use of measured transmittance data and the equation

$$\alpha_\lambda = -\frac{1}{\chi} \ln \left(\frac{\tau_\lambda}{(1 - R)^2} \right) \tag{71}$$

where

χ is the thickness of the sample

τ_λ is the percent of normal incident radiation transmitted

R is the Fresnel reflection coefficient

Our computations of spectral absorption coefficients were augmented and compared to those kindly furnished by Midwest Research Institute[2] who had occasion to compute these values while engaged in similar research. The basic source of data in each case, however, was spectral transmission curves published by Corning. A typical result of the evaluation of spectral absorption coefficient using the methods and data described appears in Figure 19.

2. Window Temperature Instrumentation

Temperatures were measured on the two faces, heat side and rear side, of each test window by electrical resistance thermometry using a fine gold film grid evaporatively deposited onto the window face. Gold was used because it is resistant to gross oxidation and has a large linear change of electrical resistance with temperature. A test window with deposited grid is shown in Figure 20. The grid pattern shown was the same for all windows tested.

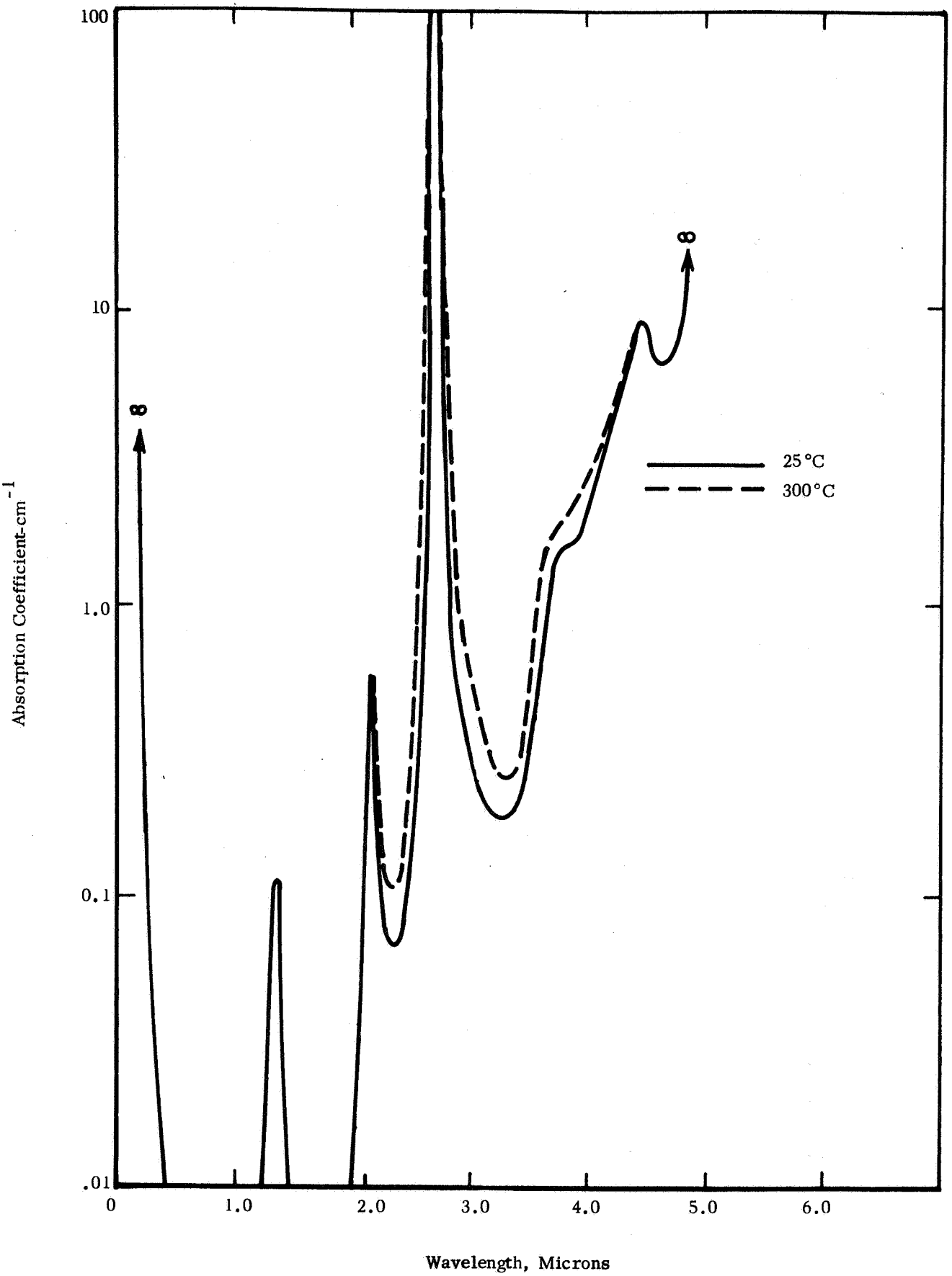

FIGURE 19 ABSORPTION COEFFICIENT VS WAVELENGTH -- FUSED SILICA, CORNING CODE NO. 7940

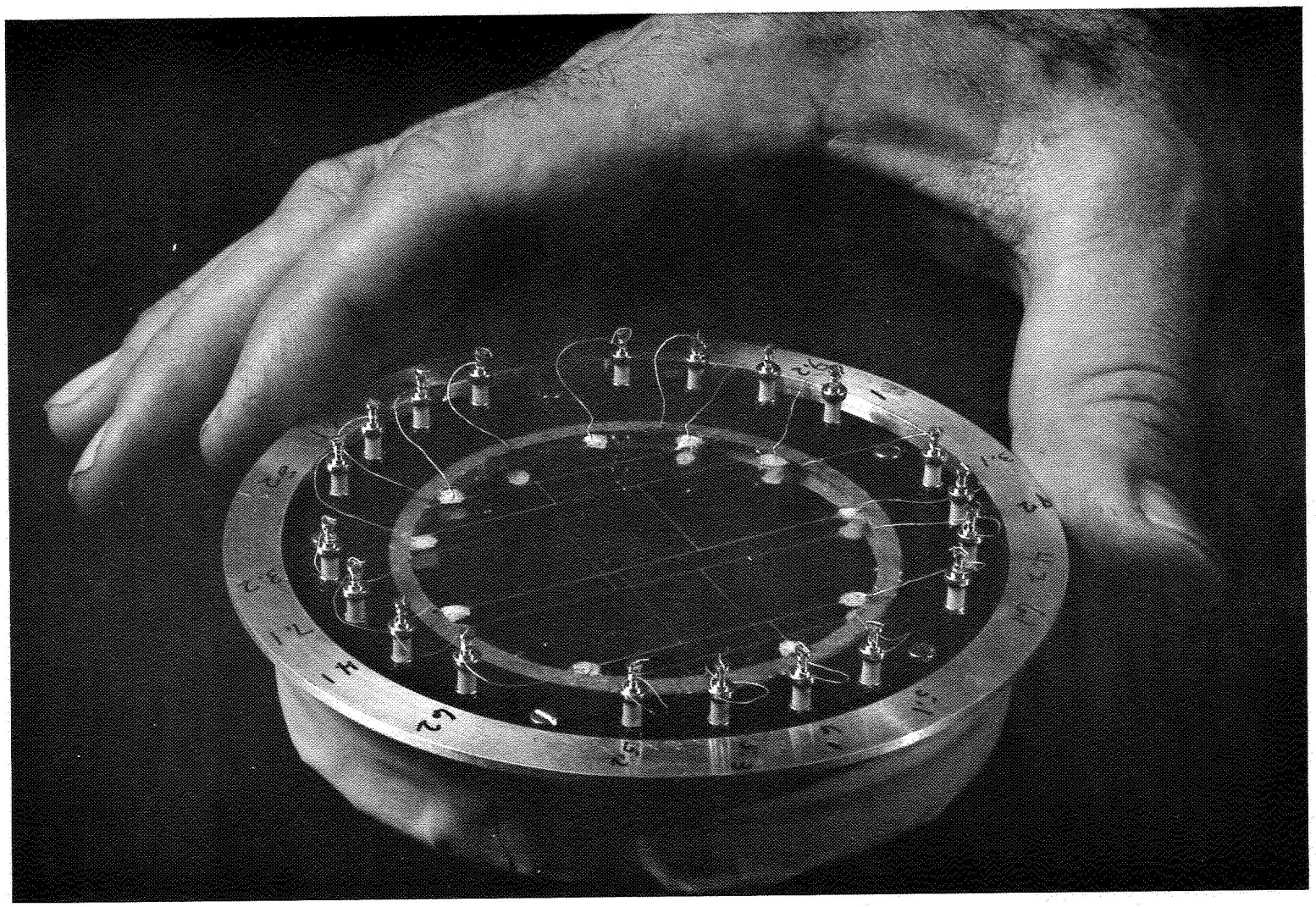

FIGURE 20 PHOTOGRAPHIC VIEW OF INSTRUMENTED TEST WINDOW

As the window was heated during a test, each of the eight sensing segments, four on each side of the window, increased their individual electrical resistances--each according to the local glass temperature and also according to the segments own temperature coefficient of resistivity. In general, these coefficients were not equal from one gold segment to the next.

The electrical resistance of four separate segments of the grid on each side of the test window was measured and recorded continuously as the measure of the window face temperatures. A small (approximately 0.5 milliampere) steady regulated current was passed through one grid path that zig-zags across the diameter of the window. Other grid paths served as voltage taps by which the electrical resistance of each sensing segment could be accurately monitored. The sensing current produced negligible ohmic heating and also was regulated sufficiently (within 0.1 percent) and held to a fixed convenient value so that the voltage tap voltages were taken directly as a measure of grid (and window) temperature at the sensing grid locations. For the most refined test results, six of eight sensors were inactivated and only two sensors were used--one at the center of the hot face of the window and one on the central rear face of the window. The temperature measuring circuits are shown in Figure 21.

The grids on each window were calibrated in an air oven against an accurate thermocouple. The instrumented test window was mounted centrally inside a heavy welded steel box with a heavy cover which was then placed centrally inside an electrically heated oven. The oven was brought to a set temperature and held there until the steel box and the sample inside it reached the same temperature. The temperature inside the steel box measured by an accurate thermocouple was taken to be the sample temperature. The grid electrical resistances were measured at the same time and recorded. Next, the oven power setting was increased to a new value and the oven allowed to reach a new equilibrium temperature plateau. We found that three to five such temperature set points including room temperature were sufficient for a complete calibration. In general, the

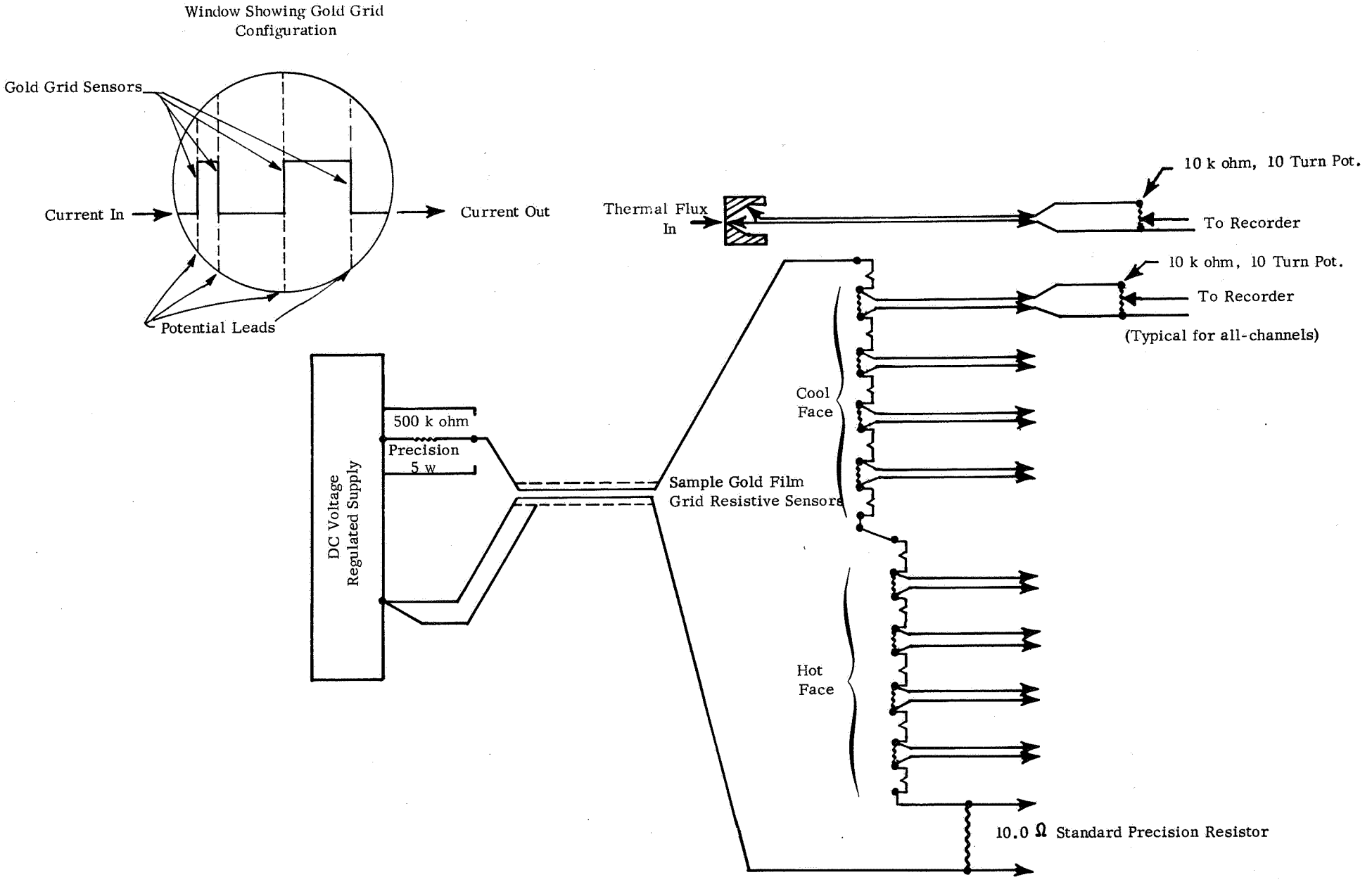

FIGURE 21 TEMPERATURE AND THERMAL IRRADIANCY MEASURING CIRCUITS

resistivity vs. temperature of each sensing segment proved to be different, even though all were evaporatively deposited together.

The application of evaporated gold grid resistance thermometry for the measurement of glass surface temperatures was developed and used successfully by Moeller and Finch [16] at Midwest Research Institute (MRI).

Taking advantage of this prior experience, an arrangement was made whereby the gold grids were evaporated onto the window samples by MRI according to ADL's pattern design, using evaporative masks cut by MRI to a grid pattern specified by ADL.

3. Window Through-Irradiance Instrumentation

The window through-irradiance is the total radiant power per unit area passing through the window. It is the sum of that directly transmitted through the window and that absorbed and re-radiated by it. The through-irradiance to be measured in these experiments was that emerging from a central area element at the back (cool) face of the window collected in a full hemisphere around the element and at all wavelengths. A Gardon-type [4] foil radiometer* was used to measure through-irradiance.

The arrangement of components involved in the irradiance measurements is illustrated in Figures 14, 15 and 22. The radiometer was brought up close to but not touching the back face of the sample window and locked in a fixed position throughout an exposure test. The spacing to the window was close, .061, so that the view factor to window material from an element on the radiometer was almost hemispherical. The radiometer was water cooled and its entire face was blackened so that the radiometer was indistinguishable, from the point of view of the window, from any of the other ambient surroundings all appearing black and at room temperature, 300°K.

---

* Product of Hy-Cal Engineering Company, Santa Fe, California, Model No. C-1300-A-10-072.

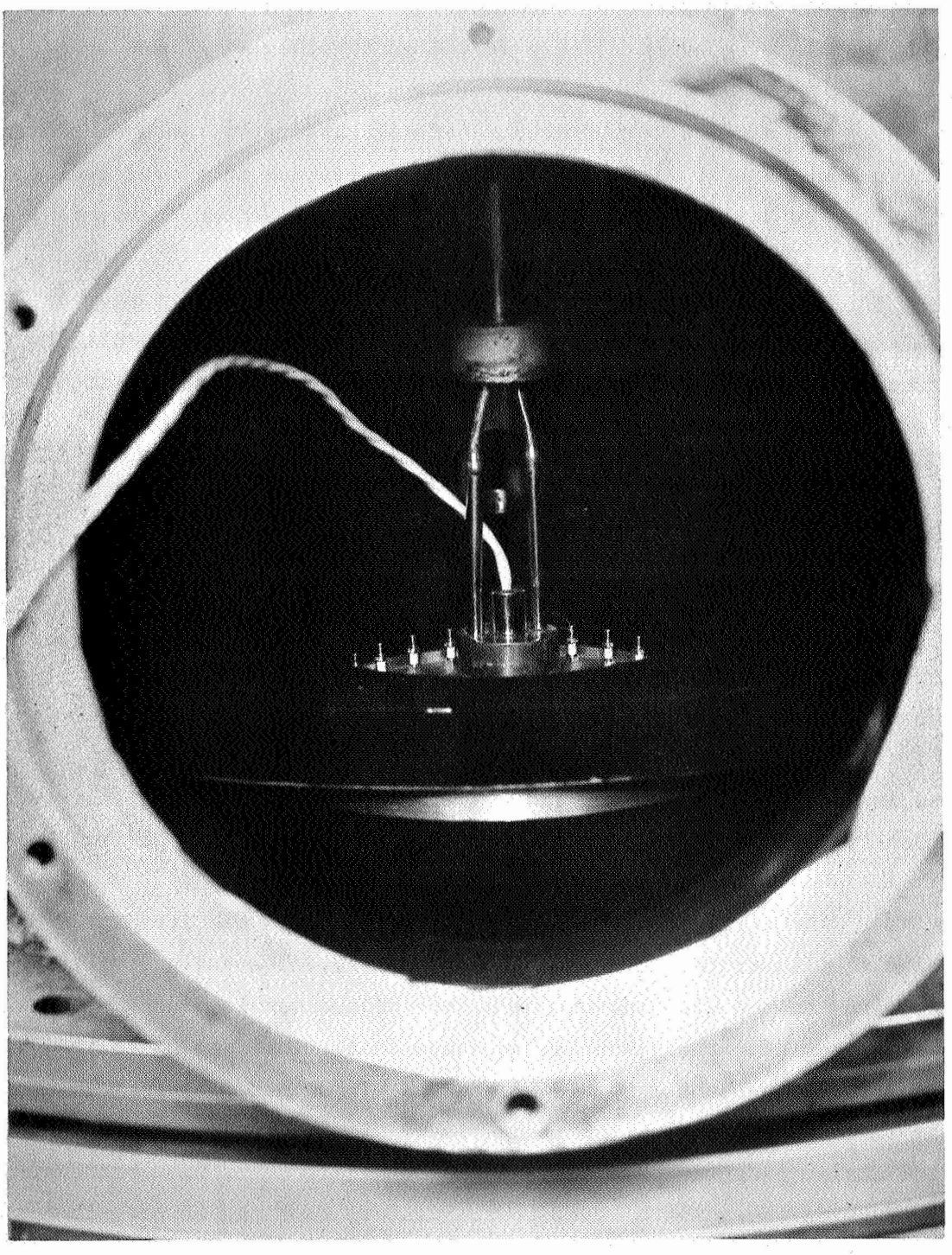

FIGURE 22 PHOTOGRAPHIC VIEW SHOWING RADIOMETER IN POSITION FOR TEST

The thermal time constant of the radiometer (less than 1 second) was negligible compared to time rates of change of window irradiance. Therefore, the radiometer output tracked accurately changes of window through-irradiance with time.

The radiometer was calibrated before each window test using the cavity as the best known (standard) source of irradiance. The calibration consisted of exposing the radiometer, positioned for a test, directly to the heated cavity source and reading its voltage output. Knowing the thermal flux leaving the cavity and the view factor to the radiometer sensing element, the radiometer sensitivity in millivolts per watt/cm^2 of thermal input was determined.

This one-point calibration technique assumes that the radiometer output voltage is linear with irradiant input. To a first approximation, such an assumption is justified on the basis of the calibration plot supplied by the manufacturer and on the basis of the theory of its operation.

Sources of error in the radiometer measurements are of three types: 1) an error due to the need to spacing the radiometer behind the window, 2) errors due to the angular dependence of radiometer absorptance, and 3) errors due to the wavelength (i.e., source temperature) dependence of radiometer absorptance.

The error due to the necessity of having a finite, practical spacing (0.061 cm set in our case) between the radiometer and window arises from the fact that the sensing element "sees" other than the central region of the test window. A correction for this effect was established experimentally by recording radiometer output vs. axial distance from the window for a typical test condition and extrapolating to zero clearance. As a result, the irradiance measurements taken at a 0.061 cm spacing were corrected by multiplying them by 1.015--this correction being so small no

further adjustments to other test circumstances were made.

In order to assess the importance of the angular dependence (non-Lambertian behavior) of the absorptance of the radiometer, a number of tests were made in which the radiometer was positioned at various distances from the cavity source when operating at a given temperature and recording the radiometer output.

The results of these tests showed that the sensitivity of the radiometer to the angle of the oncoming radiation was such that it indicated an irradiance when the oncoming radiation was confined within a 40 degree half angle about 5 percent higher than when the illumination was essentially hemispherical. This effect is consistent in direction and magnitude with that expected in the case of carbon materials.

The practical effect of this non-Lambertian behavior of the radiometer is to discriminate slightly against re-radiated radiation from the glass window which reaches the radiometer in a hemispherical distribution and to favor slightly the radiation transmitted directly through the window. This angular discrimination takes place independently of the wavelenght effects which also occur.

There appears to be no simple and rigorous way to correct for this source of experimental error since the degree of correction depends on the sample and on the fraction of incident irradiance that it re-radiates. Therefore, no correction was adopted in the data reduction process. However, this error is estimated at only a few percent and it tends toward slightly and erroneously lower through-irradiance readings for hot windows and slightly and erroneously higher through-irradiance readings for cold windows.

In order to examine the effect of the spectral distribution of the oncoming radiation on the radiometer measurement, tests were conducted in which the radiometer was set at a fixed position with respect to

the cavity and while the cavity temperature was varied over a wide range, its output was recorded. From these measurements, the sensitivity of the radiometer to source temperature was determined.

The sensitivity was found to vary several percent in temperature ranges of interest, the higher the source temperature the higher the sensitivity of the radiometer. The practical effect of this source temperature sensitivity of the radiometer is to discriminate slightly against radiation reradiated from the window at longer wavelengths and to favor slightly the directly transmitted radiation which is distributed in the shorted wavelength region.

As in the case of angular error effects there appears to be no simple and rigorous way to correct the radiometer measurements for wavelength sensitivity since the degree of correction depends on the sample itself and the fraction of incident radiation it reradiates. Thus, errors introduced by different source temperatures have not been corrected in data reduction. However, the source temperature error may be expected to lead to slightly and erroneously lower (a few percent) through-irradiance readings for hot windows and to slightly and erroneously higher through-irradiance readings for cold windows.

The magnitude of the sum of the errors due to the angular and specular dependence of the radiometer reading have been estimated roughly. An interpretation of calibration test results suggests that the radiometer discriminates slightly of the order of 10 percent against radiation generated in reradiative processes in the window and discriminates much less against radiation directly transmitted through the window.

III. MEASUREMENTS

A. GENERAL

The arrangement of test window, and test apparatus was discussed earlier in Part 3 section II and shown in Figures 14 and 15.

Experimental results are discussed elsewhere in the Summary, Part 1, for ready comparison to the computed results using the methods outlined in Part 2.

The purpose of this section is to discuss departures between experimental conditions and the conditions assumed for computation particularly with regard to one dimensionality of heat flow, to outline the experimental procedure followed in a typical test and to estimate the uncertainties involved in obtaining test data.

B. TEST GEOMETRY AND ONE-DIMENSIONALITY OF HEAT FLOW

The computer simulation of the thermal behavior of glazings deals ideally with a one-dimensional heat flow in space coordinates and a diffuse, semi-infinite source of oncoming thermal radiation--these assumptions being realistic simplifications for cases of interest. The thermal conditions achieved in the experiments approach those assumed for the analysis.

The axial location of the sample in respect to plane of the radiant cavity source was established as a compromise between the conflicting requirements of desiring to place it close to the cavity (to approach closely the condition of a semi-infinite source of oncoming radiation) and spaced away from the cavity (to allow high cavity temperatures without exceeding the structural integrity of the sample.) A third criterion was used to resolve this conflict. A statement of this criterion is that the incident angles of the source radiation received

at the center of the sample when refracted at the boundary should lie within a cone with a half angle equal to 27 degrees. This criterion establishes that all the oncoming radiation is refracted into one of the limited number of beam angles selected for computational purposes, thus, minimizing the error associated with the need to deal only with a finite number of beam angles.

The equation expressing this criterion is

$$n \sin 27^{o} = \frac{a}{\sqrt{a^2 + b^2}} \tag{72}$$

where

a is the radius of the aperture of cavity source = 3.18 cm.

b is the axial distance between the front face of the sample and the plane of the aperture of the cavity source.

n is the index of refraction of the glass sample.

The axial distance for any particular sample was established by solving this equation for b. In the case of the fused silica sample, b becomes 3.60 cm; b is equal to 3.20 cm for the aluminosilicate sample.

The flux distribution arriving from the cavity source at the sample so positioned is not uniform but axisymmetric with the form [11] shown in Figure 23. Also, heat flow from the edge of the sample is not entirely prevented although the mounting method was specially designed to reduce this flow to a reasonable minimum. For reasons of both a non-uniform flux distribution and a non-adiabatic edge condition, some radial flow takes place within the sample.

The degree to which this flow influences the comparison with computer predictions (which predictions assume a one-dimensional heat flow in space) has been considered. The effect of radial heat flow is

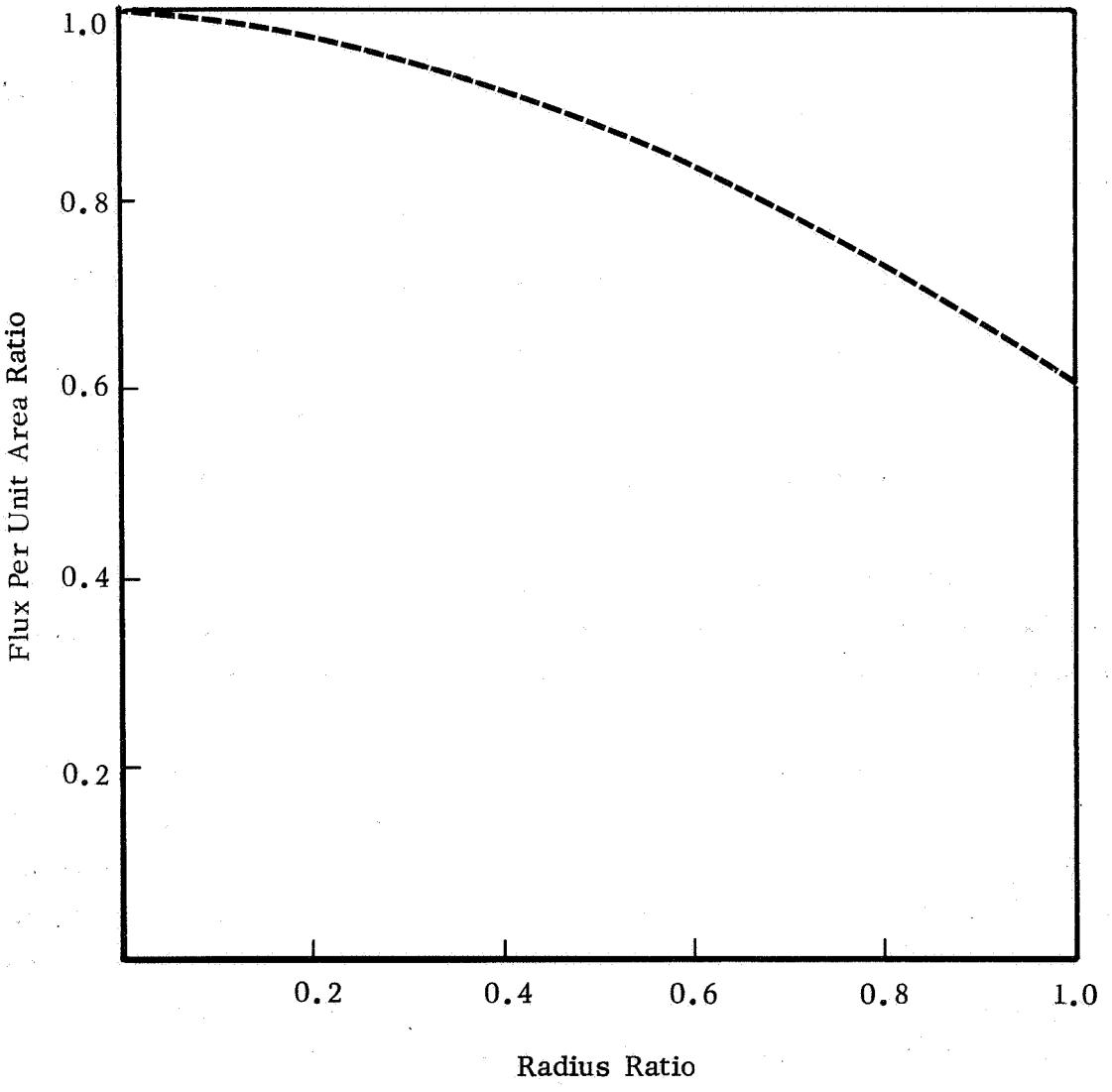

FIGURE 23 FLUX DISTRIBUTION ARRIVING AT TEST SAMPLES FROM CAVITY SOURCE

to reduce the temperature at the center of the sample and the thermal flux per unit of area leaving the back surface of the test windows relative to that which would exist under ideal conditions. An estimate of the reduction in center temperature and leaving flux has been made using the analytical methods outlined in Appendix B. For all the test conditions of our experimental program, we estimate that the sample center temperatures are reduced about 20°K at sample temperatures in the range of 500 to 900°K and the leaving flux is reduced by 0.1 to 0.2 watts/cm^2.

These estimates are based on steady-state analysis. Accordingly, they become more accurate as steady-state test conditions are approached. Nevertheless, examination of the radial temperature distributions measured in transient heating tests indicate that estimates based on the assumption of quasi steady-state conditions for radial heat flow are close enough to serve the purpose of experimental uncertainty analyses.

C. EXPERIMENTAL PROCEDURE

1. Sample Preparation

The clear quartz and aluminosilicate samples were prepared as follows: the quartz, Corning 7940, samples were cut as rough blanks from selected bubble free bulk stock by Corning Glass Works and ground on each side to clear optically flat parallel surfaces and then to circular disks by the A. D. Jones Optical Works, Burlington, Massachusetts. The aluminosilicate, Corning 1723, was prepared in the same way except from 0.95 cm thick as-rolled Corning plate. Each sample was also given 45° double bevel around its periphery to facilitate holding the sample. The sample was chemically cleaned and then heat cleaned in vacuum at 900°K and deposited with an evaporated gold temperature sensing grid identically on each side by Midwest Research Institute, Kansas City, Missouri. MRI then aged the samples in an air oven for a period of 15 hours or more at 900°K and shipped them to ADL where 5 mil silver wires were attached

to the gold grid ends using Wesgo Cement # F1312B*. The windows were then heated in an air oven for 1 hour or longer at 900°K to fire the cement. The result was a silver wire firmly bounded to both the glass window as well as the gold film. The resulting joint is shown in the photograph, Figure 20.

The samples were given a final aging at ADL for 15 hours or longer in an air oven at 900°K and were then ready for calibration.

We found in preliminary runs that incomplete aging was manifested as large unpredictable and irreversable changes in gold grid resistance. Also insufficient gold grid thickness led to grids that become electrically discontinuous after a period of high temperature exposure. With proper thickness estimated to be of the order of 1000 Angstroms or greater and with sufficient aging, the grids became stable enough temperature sensors to be useful. There was, however, a slight drift in the sensitivity of the gold grids during the test sequences for a given window, which was difficult to eliminate and which instead was accepted as an experimental error, $\pm 10^{\circ}$K.

2. Sample Calibration

Each gridded window was next calibrated in a stable high temperature air oven as described in Section II-C2.

Because the grids were found to be quite linear temperature sensors, a minimum of calibration temperature levels were required in the calibration process. We usually read grid resistance versus oven temperature at four temperatures in the region of ambient ($\simeq 300^{\circ}$K), 400°K, 600°K, and 800°K, requiring a total time of about 10 hours including cooldown.

---

*Product of Western Gold & Platinum Co., Belmont, California.

Preliminary tests had shown that residual drift in grid calibration was minimized by making the window test run shortly after calibration; i.e., within a few hours and this practice was adopted.

3. Sample Exposure Tests

The sample is mounted in its thermally isolating holding ring in the exposure apparatus; the grid silver wire leads connected up to the vacuum feedthrough circuits, the belljar lowered and sealed, the system pumped down to 10^{-5} torr, and all water cooling and electrical circuits turned on.

The sample wheel is turned such as to swing the sample away from the cavity bringing an open hole position over the cavity. Next the cavity power transformer is turned on and the saturable core controller set at a power bevel known (from previous tests) to bring the cavity to the desired temperature. About 1 hour is usually required for cavity temperature equilibrium to be reached.

The test run is begun by exposing the radiometer directly to the cavity through the open hole in the sample wheel. This exposure is typically 10 to 30 seconds. Next the sample is turned in a time less than 3 seconds to bring the sample window exactly over the cavity. The radiometer also is dropped back to exactly its previous distance from the cavity in the open hole position; i.e., the radiometer has not experienced a position changed, only the interposition of the window.

The test run consists of leaving the window in position over the cavity for longer than 300 seconds and measuring during this time the two window surface temperatures as indicated by the gold grid sensors and measuring the window through irradiance as indicated by the radiometer output.

The window is left for a period longer than the 300 second test,

1000 seconds in order to obtain data from which to estimate steady state window temperatures and irradiances.

After a run 1000 seconds later the window is swung away from the cavity and allowed to cool for 1/2 hour or so to a temperature approaching 300°K. During this time the cavity may be shut off or turned to a higher temperature setting.

Our practice was to make lower irradiance exposure tests on a given window first and higher irradiance tests last to minimize the possibility of the higher exposure disturbing the grid calibration for the low irradiance tests.

4. Data Reduction

Data was recorded on a L & N Speedomax 12 channel recorder*. All data including calibrations, run window temperatures and window through irradiances were recorded simultaneously with this recorder so that a single chart record correlated all data in time and kept it in one place. These charts are contained in ADL notebook #14255 and further data reduction recorded in ADL notebook #14518.

The temperature and irradiance chart records were curves having the appearance of the data of Figures 7 through 10 in Part 1 of this report. However, the charts are not directly readable curves in that each curve requires an individual calibration factor. Our practice was to have one person read the chart amplitude and time out loud point by point while another person looked up the corresponding true temperature on a calibration curve which included corrective factors and then record the corrected values versus time. These "true" temperature and irradiance data points were plotted to yield Figures 7 through 10 in

*Product of Leeds & Northrup Co., Dedham, Mass.

Part 1 of this report.

D. ERRORS

The errors arising in the apparatus, application of the method and instrumentation, are estimated to be as shown in Table II. The accuracy values shown are estimates of the uncertainty in the listed parameters which are involved in the measurement of window temperature and window-through irradiance. The uncertainty intervals are intended to correspond to plus or minus one to two standard deviations were it possible to conduct many sets of experiments and were it possible to know the true value of each parameter.

Precision is intended to indicate the ordinary random errors of laboratory measurements to within plus or minus one standard deviation.

The over-all error in the determination of window temperature and window through-irradiances (including the effects of uncertainties in incident irradiance) is estimated by assuming the worst case in which all the plus and all the minus uncertainty values are additive. Precision being assumed random is estimated on a root-mean-square basis.

In summary, the estimated over-all errors of these experiments are:

	Accuracy	Precision
Window temperature	$\pm$ 20°K	$\pm$ 1°K
Window through-irradiance	+ 15% - 20%	$\pm$ 3.2%

Table II

ESTIMATED ERRORS

		Factors Affecting Window Irradiance		Factors Affecting Window Temperature	
	Parameter Range	Accuracy	Precision	Accuracy	Precision
1. Cavity temperature	1125°K & 1300°K	±10°K, ±1%	±2°K		
Total Hemispherical Emittance, ε_a	.946	±3%			
Total Normal Emittance	.946	±3%			
Irradiance	≃4 watt/cm^2 & 7 watt/cm^2 at window	±7%	±1%		
2. Window temperature	≃650°K to ≃750°K			±10°K, ±1.5%	±3°K, ±.25%
Through-Irradiance	≃1 watt/cm^2 to ≃4 watt/cm^2	+5% -10%	±3%		
Ambient (300°K) Irradiance	≃5 x 10^{-2} watt/cm	±1% of lowest irradiance			
3. Mechanical Cavity-window Distance	3 cm to 9 cm	±.5%			
Aperture Diam., rigidity of fixtures, etc.					
4. Electronic & Electrical Drifts & Errors	-	±.5%	±.1%	±.5%	±.1%
5. Data Reading & Reduction	-	±1%	±.5%	±1%	±.5%
TOTAL ERRORS		+15% -20%	σ = 3.2%	±20°K, ±3%	σ = 0.6%

Arthur D. Little, Inc.

APPENDIX A

CORRECTIONS FOR OPTICAL PYROMETER READINGS

A pyrometer operating at pyrometer red ($\lambda = .65 \times 10^{-4}$ cm) indicates a blackbody temperature denoted by a prime, T', which is lower than the true temperature, T, of the object (cavity) due to the fact that the objects emittance ε_λ as well as intervening elements, such as a chamber window, reduce the objects brightness by a factor k. The factor k is 1.00 for a blackbody object with no intervening window and less than 1.00 for a non-black emittance and/or intervening windows.

The Planck equation for a non-black radiating object is

$$W_\lambda = kC_1\lambda^{-5} \left(e^{\frac{C2}{\lambda T}} - 1\right)^{-1} \qquad \text{(A1)}$$

and

$$k = \varepsilon_\lambda \tau_\lambda \qquad \text{(A2)}$$

where

W_λ = spectral radiance of the object
k = the reduction factor defined above
C_1 = first Planck constant = 3.74×10^{-12} watt-cm^2
C_2 = second Planck constant = 1.438 cm°K
λ = wavelength, cm
e = naperian base
T' = pyrometer indicated blackbody temperature of object, °K
T = true temperature of object, °K
ε_λ = spectral emittance at $\lambda = .65 \times 10^{-4}$ cm
τ_λ = spectral transmittance of intervening window
$R = \left(\frac{1-n}{1+n}\right)^2$
n = spectral index of refraction

Introducing Wein's law as an adequate approximation of Planck's law and the approximation $T \simeq T'$, then

$$T - T' = - \frac{\lambda}{C_2} (T')^2 \ln k \qquad \text{(A3)}$$

Equation (A3) gives the temperature correction T-T' to be added to a pyrometer reading T' to arrive at an estimated true temperature of the object T.

As an example for transmission of radiation in the spectral band of pyrometer red ($\lambda = 0.65 \times 10^{-4}$ cm) through a clear Vycor window of

$$\tau_\lambda = 1\text{-}2\ (0.035) = 0.93$$

and for a cavity angular spectral emittance at $\lambda = 0.065 \times 10^{-4}$ cm of

$$\varepsilon_\lambda = 0.95$$

and for a temperature of 1300°K, the solution of equation (A3) gives

$$T - T' = 7°K$$

APPENDIX B

ESTIMATING TWO-DIMENSIONAL FLOW EFFECTS IN TEST SAMPLES

Consider the problem of steady-state heat flow in a glass disk receiving radiant thermal power on one face and reradiating to cold black surroundings. The impinging thermal energy varies as a function of radius but is axisymmetric. Heat in amount q_a flows out the edge of the sample, that is, at radius r equal to a.

The differential equation describing the temperature distribution in the sample is

$$\frac{d^2T}{dr^2} + \frac{1}{r}\frac{dT}{dr} + \frac{1}{K\delta}\left[q(r) - 2\varepsilon\sigma T^4\right] = 0 \qquad \text{(B1)}$$

where

T is the temperature at radial location r

K is the coefficient of thermal conductivity

q(r) is the absorbed radiant flux at radius r

ε is the effective emissivity of the sample

σ is the Stefan-Boltzmann constant

To solve equation (B1), we first linearize about the temperature T_o; i.e., we let $T = T_o + \Theta$ which transforms equation (B1) to

$$\frac{d^2\Theta}{dr^2} + \frac{1}{r}\frac{d\Theta}{dr} - \alpha^2\Theta = -\frac{1}{K\delta}\left[q(r) - 2\sigma T_o^4\right] \qquad \text{(B2)}$$

where

$$\alpha^2 = \frac{8\varepsilon\sigma T_o^3}{K\delta}$$

A solution to this equation which satisfies the boundary conditions of our problem including a close approximation to the flux distribution q(r) presented to the sample under test conditions is

$$\theta = C_1 I_o (\alpha r) + \theta_o J_o \left(\beta \frac{r}{a}\right) \tag{B3}$$

where

$$C_1 = \frac{\frac{-q_a}{2\pi a K \delta} + \theta_o \frac{\beta}{a} J_1 (\beta)}{\alpha I_1 (\alpha a)} \tag{B4}$$

J_o is Bessel function of the first kind

I_o and I_1 are modified Bessel functions

β is first root of J_o and is equal to 2.405

and

$$\theta_o = \frac{\Delta q}{K\delta\left[\left(\frac{\beta}{a}\right)^2 + \alpha^2\right]} \tag{B5}$$

where

Δq is the difference in the radiant flux absorbed at $r = o$ and $r = a$.

Δq is related to the flux absorbed at the center of the sample by

$$\Delta q = b q_c \simeq 2b\varepsilon\sigma T_c^{\,4} \tag{B6}$$

where

T_c is the temperature of the sample at $r = o$

b is a constant descriptive of the flux distribution

The center temperature for a sample uniformly irradiated with an adiabatic edge condition is given by

$$2\varepsilon\sigma T_c^{\,4} = q_c \tag{B7}$$

The center temperature for a sample under test conditions is given by a rearrangement of equation (B1)

$$2\varepsilon\sigma T_c^{\,4} = q_c + K\delta \left(\frac{d^2\theta}{dr^2} + \frac{1}{r}\frac{d\theta}{dr}\right)\Bigg|_{r=o} \tag{B8}$$

Computing the derivatives $\frac{d^2\Theta}{dr^2}$ and $\frac{1}{r}\frac{d\Theta}{dr}$ from equation (B3) and substituting in equation (B8), we get

$$2\varepsilon\sigma T_c^4 = q_c + K\delta\left[C_1\alpha^2 - \Theta_o\left(\frac{\beta}{a}\right)^2\right] \tag{B9}$$

The difference in center temperature due to non-uniform flux and edge heat flow is, therefore, given by

$$2\varepsilon\sigma\Delta(T_c^4) = K\delta\left[C_1\alpha^2 - \Theta_o\left(\frac{\beta}{a}\right)^2\right]$$

or

$$\Delta T_c \simeq \frac{K\delta\left[C_1\alpha^2 - \Theta_o\left(\frac{\beta}{a}\right)^2\right]}{8\varepsilon\sigma T_c^3} \tag{B10}$$

As an example of the use of the developed equations, consider a fused silica test sample 0.635 cm thick irradiated such that it operates at a nominal temperature of 800°K. It is mounted in such a fashion that the heat flowing out its edge must pass through .318 cm of Min-K* high temperature insulation to a mounting plate maintained at 300°K.

Constants of the problem are:

$K = 1.85 \times 10^{-2}$ watt/cm-°K

$\delta = 0.635$ cm

$K\delta = 1.18 \times 10^{-2}$ watt/°K

K_k (thermal conductivity of Min-K) $= 4 \times 10^{-4}$ watt/cm-°K

c (thickness of Min-K) = .318 cm

a = 3.17 cm

$q_a = 2\pi a\delta K_k \frac{\Delta T}{c} = 7.95$ watts

b = 0.4

---

* Product of Johns-Manville Aerospace Products.

$$\alpha^2 = \frac{8\varepsilon\sigma T_o^3}{K\delta} = 2 \text{ cm}^{-2}$$

$$\alpha a = 4.5$$

$$I_o(\alpha a) = 17.5$$

$$I_1(\alpha a) = 15.4$$

$$\Delta q = 2b\varepsilon\sigma T_c^4 = 1.84 \text{ watt/cm}^2$$

from equation (B5)

$$\Theta_o = 60.5°K$$

from equation (B4)

$$C_1 = 0.45°K$$

from equation (B10)

$$\Delta T_c = 17.1°K$$

Commensurate with this 17.1°K reduction in center temperature, the thermal flux per unit area leaving the back surface of the window test sample is reduced by 0.2 watt/cm^2.

APPENDIX C

REFERENCES

1. Charnock, H., "Experimental and Theoretical Comparison of Radiation Conductivity Predicted by Steady-State Theory with that Effective under Periodic Temperature Conditions," J. Am. Cer. Soc., 44, 313-317 (1961).

2. Finch, H. L., personal correspondence, November 11, 1965.

3. Finch, H. L. et al, "Experimental Verification of the Analyses and Computer Programs Concerning Heat Transfer through Semitransparent Materials,"AFFDL-TR-65-136, July 1965.

4. Gardon, R., "An Instrument for the Direct Measurement of Intense Thermal Radiation," Rev. of Sc. Intr., 24, No. 5, May 1953.

5. Gardon, R., "The Emissivity of Transparent Materials," J. Am. Cer. Soc. 39, 278-287, (1956), Volume 44.

6. Gardon, R., "Calculation of Temperature Distributions in Glass Plates Undergoing Heat Treatment," J. Am. Cer. Soc., 41, 200-209 (1958).

7. Gardon, R., "A Review of Heat Transfer in Glass" J. Am. Cer. Soc., 44, 305-312 (1961).

8. Gardon, R., "On the Apparent Thermal Conductivity of Diathermanous Materials," Second Conference on Thermal Conductivity, Ottawa Canada, October 10-12, 1962.

9. Grove, F. J., "Spectral Transmission of Glass at High Temperatures and Its Application to Heat-Transfer Problems," J. Am. Cer. Soc. 44, 317-320 (1961).

10. Grove, F. J and Jellyman, P. E., "The Infra-red Transmission of Glass in the Range Room Temperature to 1400°," Jour. Soc. Glass Tech., 34, 3T-15T (1955).

11. Hamilton, D. C. and Morgan, W. R., "Radiant-Interchange Configuration Factors," NACA TN 2836 (1952).

12. Kellett, B. S., "The Steady Flow of Heat through Hot Glass," J.O.S.A., 42, 339-343 (1952).

13. Kingery, W. D., "Heat-Conductivity Processes in Glass," J. Am. Cer. Soc., 44, 302-304 (1961).

14. Lis, S. J., et al, "Investigation of Window System Configuration Concepts for Advanced Aerospace-Vehicles," Technical Report ASD-TR-63, October 1963.

15. McMahon, H. O., "Thermal Radiation from Partially Transparent Reflecting Bodies," J.O.S.A., 40, 376-380 (1950).

16. Moeller, C. E., and Finch, H. L., "Transparent Boundary Apparatus for Determining Heat Flow through Glass," Fourth Conference on Thermal Conductivity, San Francisco, October 13-16, 1964.

17. Neuroth, N. Von, "Der Temperatureinfluss auf die Optischen Konstanten von Glas im Gebiet Starher Absorption," Glastechnische Berichte, 28 Jahrgang (1955).

18. Nixon, J. A. and Monroe, S. G., "Heat Transfer through Diathermanous Materials," J. Spacecraft, Volume 2, No. 6, November-December 1965.

19. Plunkett, J. D. and Kingery, W. D., "The Spectral and Integrated Emissivity of Carbon and Graphite," Proc. of the Forth Conf. on Carbon, Pergamon Press, New York (1960).

20. Reitzel, J., "Infrared Spectra of SiO_2 from 400 to 600 cm^{-1}," J. Chem. Phys., 23, 2407-2409 (1955).

21. Schuster, A., "Radiation through a Foggy Atmosphere," Astrophys. J., 21, (1905).

22. Sparrow, E. M. and Jonsson, V. K., "Absorption and Emission Characteristics of Diffuse Spherical Enclosures," Jour. of Heat Trans. ASME, May 1960.

23. Strong, P. F. and Emslie, A. G., "The Method of Zones for the Calculation of Temperature Distribution," ASME 65-WA/HT-47 (1965).

24. Wray, K. L. and Connolly, T. J., "Thermal Conductivity of Clear Fused Silica at High Temperatures," J. App. Phys., 30, 1702-1705 (1959).